

3-2015

Electrical and Physical Property Characterization of Single Walled Carbon Nanotube Ink for Flexible Printed Electronics

Kristian E. Warner Jr.

Follow this and additional works at: <https://scholar.afit.edu/etd>



Part of the [Electrical and Computer Engineering Commons](#), and the [Nanoscience and Nanotechnology Commons](#)

Recommended Citation

Warner, Kristian E. Jr., "Electrical and Physical Property Characterization of Single Walled Carbon Nanotube Ink for Flexible Printed Electronics" (2015). *Theses and Dissertations*. 66.
<https://scholar.afit.edu/etd/66>

This Thesis is brought to you for free and open access by the Student Graduate Works at AFIT Scholar. It has been accepted for inclusion in Theses and Dissertations by an authorized administrator of AFIT Scholar. For more information, please contact AFIT.ENWL.Repository@us.af.mil.



**ELECTRICAL AND PHYSICAL PROPERTY CHARACTERIZATION OF
SINGLE WALLED CARBON NANOTUBE INK FOR FLEXIBLE PRINTED
ELECTRONICS**

THESIS

Kristian E. Warner Jr, Second Lieutenant, USAF

AFIT-ENG-MS-15-M-066

**DEPARTMENT OF THE AIR FORCE
AIR UNIVERSITY**

AIR FORCE INSTITUTE OF TECHNOLOGY

Wright-Patterson Air Force Base, Ohio

**DISTRIBUTION STATEMENT A:
APPROVED FOR PUBLIC RELEASE; DISTRIBUTION UNLIMITED**

The views expressed in this thesis are those of the author and do not reflect the official policy or position of the United States Air Force, the Department of Defense, or the United States Government.

This material is declared a work of the U.S. Government and is not subject to copyright protection in the United States.

AFIT-ENG-MS-15-M-066

ELECTRICAL AND PHYSICAL PROPERTY CHARACTERIZATION OF SINGLE
WALLED CARBON NANOTUBE INK FOR FLEXIBLE PRINTED ELECTRONICS

THESIS

Presented to the Faculty
Department of Electrical and Computer Engineering
Graduate School of Engineering and Management
Air Force Institute of Technology
Air University
Air Education and Training Command
in Partial Fulfillment of the Requirements for the
Degree of Master of Science in Electrical Engineering

Kristian E. Warner Jr, BS
Second Lieutenant, USAF

March 2015

DISTRIBUTION STATEMENT A:
APPROVED FOR PUBLIC RELEASE; DISTRIBUTION UNLIMITED

AFIT-ENG-MS-15-M-066

ELECTRICAL AND PHYSICAL PROPERTY CHARACTERIZATION OF SINGLE
WALLED CARBON NANOTUBE INK FOR FLEXIBLE PRINTED ELECTRONICS

THESIS

Kristian E. Warner Jr, BS
Second Lieutenant, USAF

Committee Membership:

Maj Derrick Langley, PhD
Chair

Dr. Carrie M. Bartsch
Member

Dr. Ronald Coutu
Member

Dr. Mary Y. Lanzerotti
Member

Abstract

This research presents a method of characterizing single-walled carbon nanotube (SWCNT) ink. This research also examines the results of our characterization efforts. First, the process of ink jet printing SWCNT ink onto organic and inorganic substrates is discussed. Next, the tests for measuring sheet resistance, conductance, inductance, adherence, thickness, roll-off, and S-parameters of the ink are described. Results and findings of the research are presented. The SWCNT ink created by Brewer Science © is shown to be an effective material for additive manufacturing using an aerosol jet printer, but not an inkjet printer. The ink is shown to have a sheet resistance on the order of $5\text{ }k\Omega/\square$. The thickness is shown to be between 50 and 800 nm. An inductor is printed and shown to have an inductance on the order of $1\text{ }\mu H$. Future research directions are discussed, including the additional characterization of SWCNT ink.

Acknowledgments

I would like to acknowledge and thank my advisors, Dr. Mary Lanzerotti and Maj Derrick Langley, as well as the other members of my thesis committee, Dr. Carrie Bartsch and Dr. Ronald Coutu, for their help, support, and guidance proffered while I conducted this research. I would also like to acknowledge Dr. Eric Kreit for running the aerosol jet printer and Mr. Will Gouty for his assistance with the COSMOS network analyzer. Additionally, I would like to thank Mr. Brad Paul for sponsoring my entrance to NAECON 2014 and Dr. Emily Heckman and Dr. Carrie Bartsch for their efforts in leading the Printronics Laboratory. Finally, I would like to acknowledge and thank my wife for her tremendous patience in supporting my education.

Kristian E. Warner Jr

Table of Contents

| | Page |
|--|------|
| Abstract | iv |
| Acknowledgments | v |
| Table of Contents | vi |
| List of Figures | x |
| List of Tables | xiv |
| List of Acronyms | xv |
| I. Introduction | 1 |
| 1.1 General Issue | 1 |
| 1.2 Problem Statement | 2 |
| 1.3 Research Objectives, Questions, and Hypotheses | 2 |
| 1.3.1 Research Objectives | 2 |
| 1.3.2 Investigative Questions | 2 |
| 1.3.3 Hypotheses | 3 |
| 1.4 Research Focus | 5 |
| 1.5 Methodology | 5 |
| 1.6 Assumptions and Limitations | 5 |
| 1.7 Significance | 6 |
| II. Literature Review | 7 |
| 2.1 Chapter Overview | 7 |
| 2.2 Description | 7 |
| 2.3 Relevant Research | 8 |
| 2.3.1 Carbon Nanotube Background | 8 |
| 2.3.1.1 Electrical, Thermal, and Optical Characteristics of Carbon Nanotubes | 8 |
| 2.3.1.2 Structure of Carbon Nanotubes | 9 |
| 2.3.2 Cooling | 9 |
| 2.3.2.1 Methodology | 10 |
| 2.3.2.2 Utilization | 10 |
| 2.3.3 Dense Carbon Nanotube (CNT) Arrays | 11 |

| | Page |
|---|--------|
| 2.3.3.1 Methodology | 12 |
| 2.3.3.2 Utilization | 12 |
| 2.3.4 Sensing | 13 |
| 2.3.4.1 Methodology | 13 |
| 2.3.4.2 Utilization | 14 |
| 2.3.5 Photoreaction | 15 |
| 2.3.5.1 Methodology | 15 |
| 2.3.5.2 Utilization | 15 |
| 2.3.6 Semiconductors | 16 |
| 2.3.6.1 Methodology | 16 |
| 2.3.6.2 Utilization | 17 |
| 2.3.7 Printed Electronics | 18 |
| 2.3.7.1 Printed Organic Field Effect Transistor (FET)s | 18 |
| 2.3.7.2 Electronic and Structural Printer | 19 |
| 2.3.8 Printronics Laboratory Research | 20 |
| 2.3.8.1 Printed Photodetectors on Paper Substrates | 20 |
| 2.3.8.2 Biotronics and Salmon Waste as Ink | 20 |
| 2.3.8.3 Bio-Organic FETs | 21 |
| 2.3.9 Feasibility of Printed Radio Frequency Identification (RFID) Circuits | 23 |
| 2.3.9.1 All-Printed RFID Circuits | 25 |
| 2.3.9.2 Future Research | 26 |
| 2.3.10 Inkjet Printing Techniques | 26 |
| 2.3.10.1 Factors Which Affect Inkjet Printing | 26 |
| 2.3.10.2 Effects of Overwriting and Line Width | 29 |
| 2.3.11 Aerosol Jet Printing | 31 |
| 2.4 Summary | 32 |
| III. Methodology | 33 |
| 3.1 Chapter Overview | 33 |
| 3.2 Experimental Methodology | 33 |
| 3.2.1 Initial Test Methodology | 33 |
| 3.2.1.1 Length and Chirality | 34 |
| 3.2.1.2 Ink Solvent Characteristics | 34 |
| 3.2.1.3 Ink Particulate Suspension | 34 |
| 3.2.1.4 Environmental Variables | 36 |
| 3.2.1.5 Ink Failure | 36 |
| 3.2.2 Primary Test Methodology | 37 |
| 3.2.2.1 DC Test Measurements and Equipment | 37 |
| 3.2.2.2 RF Test Measurements and Equipment | 38 |
| 3.2.2.3 Mechanical Test Measurements and Equipment | 39 |
| 3.2.2.4 Testing | 39 |

| | Page |
|---|--------|
| 3.3 Test Subjects | 40 |
| 3.3.1 Lines | 40 |
| 3.3.2 Rectangles | 40 |
| 3.3.3 Coplanar Waveguides | 41 |
| 3.3.3.1 Coplanar Waveguide (CPW) with Silver | 42 |
| 3.3.4 Inductors | 44 |
| 3.4 Summary | 44 |
| IV. Analysis and Results | 46 |
| 4.1 Chapter Overview | 46 |
| 4.2 Results of Experimentation | 46 |
| 4.2.1 Viability of Substrates | 46 |
| 4.2.1.1 Paper | 46 |
| 4.2.1.2 Glass | 47 |
| 4.2.1.3 Polyimide | 48 |
| 4.2.1.4 Nomex © | 49 |
| 4.2.2 Thickness of Deposited Ink | 49 |
| 4.2.3 Sheet Resistance | 50 |
| 4.2.3.1 Resistivity and Sheet Resistance | 51 |
| 4.2.3.2 Resistivity of Aerosol Jet Printed Ink | 52 |
| 4.2.3.3 Conductivity | 52 |
| 4.2.4 S-parameters | 52 |
| 4.2.4.1 Effect of Thermal Bias on S-parameters | 57 |
| 4.2.4.2 Effect of Electric Field Bias on S-parameters | 57 |
| 4.2.5 Fourier Transform Infrared Spectroscopy | 57 |
| 4.2.6 Inductance | 60 |
| 4.2.7 Viability of the Brewer Science © CNT-based Ink | 61 |
| 4.2.8 Test Subjects by Reference Number | 62 |
| 4.3 Summary | 65 |
| V. Conclusions and Recommendations | 67 |
| 5.1 Chapter Overview | 67 |
| 5.2 Investigative Questions Answered | 67 |
| 5.2.1 Previously Answered Investigative Questions | 67 |
| 5.2.2 Unanswered Investigative Question | 68 |
| 5.3 Conclusions of Research | 68 |
| 5.4 Significance of Research | 69 |
| 5.5 Recommendations for Future Research | 69 |
| 5.6 Summary | 70 |

Page

Bibliography 71

List of Figures

| Figure | Page |
|---|------|
| 1.1 Hypothesized dependence of electrical characteristics on deposited ink thickness. | 4 |
| 2.1 Bonding schemes for noble and oxidizing metals [17] | 11 |
| 2.2 CNT arrays. (a) shows a forest of CNTs. (b) shows a forest of CNTs grown using Robertson's method. [18] | 12 |
| 2.3 e-Whisker production diagram [20] | 13 |
| 2.4 e-Whisker utilization diagram [20] | 14 |
| 2.5 Single Walled Carbon Nanotube (SWCNT) photoreactor utilization diagram. 2.5(a) shows construction and actuation of a SWCNT photoreactor; 2.5(b) shows a photograph of a SWCNT photoreactor; 2.5(c) shows time lapse photographs of a bending SWCNT photoreactor; 2.5(d) shows bending angle as a function of time for multiple wavelengths of light; 2.5(e) shows maximum bending angle as a function of white light intensity [21]. | 16 |
| 2.6 Single walled carbon nanotube encapsulating a graphene ribbon [24] | 17 |
| 2.7 Printed temperature sensor with rewritable memory and screen [27] | 18 |
| 2.8 Ink jet process for printing a flexible FET [26] | 19 |
| 2.9 Photodetector device cross-subsection with material energy levels (a); two PDs on paper substrate (b); poly(3,4-ethylenedioxythiophene):poly(styrenesulfonate) (PEDOT:PSS) when printed directly on poly(3-hexylthiophene):C61-butyrat acid methyl ester (P3HT:PCBM) (c); PEDOT:PSS on P3HT:PCBM with a deoxyribonucleic acid (DNA) interlayer (d) [28]. | 21 |
| 2.10 I-V characteristics of the photodetector in the dark (a); photodetector response to light pulses (b); photodetector response to light pulses under applied voltage (c); photodetector response frequency dependence at 525 nm wavelength [28]. | 22 |

| Figure | Page |
|---|------|
| 2.11 Performance of a DNA-based Bio-organic FET (bioFET). 2.11(a) shows the layout of an n-type bioFET device; 2.11(b) shows the output characteristics of an n-type DNA-based bioFET device; 2.11(c) shows an n-type bioFET's transfer characteristics for the given voltage; 2.11(c) inset shows an n-type bioFET's transfer characteristics for the given voltage when non-crosslinked DNA is used [30]. | 23 |
| 2.12 Performance of a DNA-based bioFET. 2.12(a) shows the layout of a p-type bioFET device; 2.12(b) shows the output characteristics of a p-type DNA-based bioFET device; 2.12(c) shows a p-type bioFET's transfer characteristics for the given voltage; 2.12(c) inset shows a p-type bioFET's transfer characteristics for the given voltage when non-crosslinked DNA is used [30]. | 24 |
| 2.13 A printed RFID tag on flexible substrate [35]. | 25 |
| 2.14 Substrate treatment effects on contact angle and CNT dispersion. (a) shows drop contact angle on glass; (b) shows drop contact angle on treated glass; (c) and (d) show drops (a) and (b) after drying [36]. | 27 |
| 2.15 Substrate temperature effects on drying time and CNT dispersion. (a) shows CNT dispersion and drying time for room temperatures; (b) shows CNT dispersion and drying time for heated substrates [36]. | 28 |
| 2.16 Overwriting effects on CNT network formation. (a) shows the CNT network formed after a single printed drop; (b) shows the CNT network formed after two drops; (c) shows the CNT network formed after five drops; (d) shows the CNT network formed after eight drops [36]. | 30 |

| Figure | Page |
|--|------|
| 2.17 Overwriting and line width effects on CNT transparency. (a) shows the effect of overwriting and line width on transparency; (b) shows a printed CNT circuit on glass [36]. | 31 |
| 2.18 Overwriting effects on resistivity and thickness with line width effects on I-V characteristics. Fig. (a) shows the effect of overwriting on resistivity and thickness; Fig. (b) shows the I-V characteristics of printed CNT lines with varying widths [36]. | 32 |
| 3.1 Functionalization of CNTs in solution via addition of surfactant. (a) shows a cross section of a surfactant-functionalized CNT; (b) shows the side view of the same CNT [41]. | 35 |
| 3.2 Effects of surfactant on drop surface tension. (a) shows a $3 \mu\text{L}$ drop of water on SiO_2 substrate ; (b) shows a $3 \mu\text{L}$ drop of water with surfactant on SiO_2 substrate [41]. | 36 |
| 3.3 Schematic of a four-point probe. A represents the current flowing through probes 1 and 4; V represents the voltage across probes 2 and 3 [46]. | 38 |
| 3.4 Printed line on polyimide. | 41 |
| 3.5 Printed square on paper. | 42 |
| 3.6 A standard CPW with a juxtaposed axis system [50]. | 43 |
| 3.7 Printed CPW on paper. | 43 |
| 3.8 A square spiral inductor. | 44 |
| 4.1 Sheet resistance of printed lines on paper. | 51 |
| 4.2 Sheet resistance of printed lines on Nomex ©. | 51 |
| 4.3 Rectangular chart plot of $S[1,1]$ for sample 35, a CPW of 9 layers. | 54 |
| 4.4 Smith chart plot of $S[1,1]$ for sample 35, a CPW of 9 layers. | 54 |

| Figure | Page |
|---|------|
| 4.5 Rectangular chart plots of S-parameters for CPWs printed with an aerosol jet printer. CNT 1 represents a CPW with a thickness of 300 nm. CNT 1 outside, CNT 1 inner, and CNT 1 midway are plots from a single CPW with a thickness of 780 nm. CNT 1 outside represents measurements taken across the full length of the CPW. CNT 1 midway represents measurements taken across half of the CPW. CNT 1 inner represents measurements taken across a minimal distance of the CPW. | 55 |
| 4.6 Smith chart plots of S-parameters for CPWs printed with an aerosol jet printer. CNT 1 represents a CPW with a thickness of 300 nm. CNT 1 outside, CNT 1 inner, and CNT 1 midway are plots from a single CPW with a thickness of 780 nm. CNT 1 outside represents measurements taken across the full length of the CPW. CNT 1 midway represents measurements taken across half of the CPW. CNT 1 inner represents measurements taken across a minimal distance of the CPW. | 56 |
| 4.7 Fourier Transform Infrared Spectroscopy (FTIR) data for the Brewer Science © CNT-based ink. | 58 |
| 4.8 SEM image under 50kX magnification of CNT ink printed on silicon nitride coated silicon using the aerosol jet printer. | 59 |
| 4.9 SEM image under 250kX magnification of CNT ink printed on silicon nitride coated silicon using the aerosol jet printer. | 60 |

List of Tables

| Table | | Page |
|-------|---|------|
| 1.1 | Bulk Conductivity of Metals and CNTs [4] [5] | 3 |
| 4.1 | Surface Roughness of Paper, Glass, Polyimide, and Nomex © | 50 |
| 4.2 | Thickness and Series Inductance and Resistance of Printed Inductors on Glass. | 61 |
| 4.3 | Detailed Parameters for All Printed Test Subjects. | 63 |
| 4.4 | Detailed Parameters for All Printed Test Subjects, Part 2. | 64 |
| 4.5 | Detailed Parameters for All Printed Test Subjects, Part 3. | 65 |

List of Acronyms

| Acronym | Definition |
|-----------|---|
| AFRL | Air Force Research Laboratory |
| APS | aminopropyl-trialkoxy-silane |
| bioFET | Bio-organic FET |
| CNT | Carbon Nanotube |
| COTS | Commercial, Off-The-Shelf |
| CPW | Coplanar Waveguide |
| CTMA | hexadecyltrimethylammonium chloride |
| DNA | deoxyribonucleic acid |
| DoD | Department of Defense |
| DoE | Department of Energy |
| FET | Field Effect Transistor |
| FE-SEM | Field Emission - Scanning Electron Microscope |
| FTIR | Fourier Transform Infrared Spectroscopy |
| HMDS | hexamethyldisilazane |
| LBNL | Lawrence Berkeley National Laboratory |
| LCR | Inductance-Capacitance-Resistance |
| MSD | Materials Sciences Division |
| NBMC | Nano Bio Manufacturing Consortium |
| NFET | n-Type Field Effect Transistor |
| P3HT:PCBM | poly(3-hexylthiophene):C61-butyric acid methyl ester |
| PEDOT:PSS | poly(3,4-ethylenedioxythiophene):poly(styrenesulfonate) |
| PFET | p-Type Field Effect Transistor |
| PDMS | Polydimethylsiloxane |

| Acronym | Definition |
|---------|--------------------------------|
| SEM | Scanning Electron Microscope |
| SWCNT | Single Walled Carbon Nanotube |
| VLSI | Very Large Scale Integration |
| RFID | Radio Frequency Identification |
| TCF | Transparent Conductive Film |
| TFT | thin film transistor |
| USAF | United States Air Force |

ELECTRICAL AND PHYSICAL PROPERTY CHARACTERIZATION OF SINGLE WALLED CARBON NANOTUBE INK FOR FLEXIBLE PRINTED ELECTRONICS

I. Introduction

This chapter introduces the research contained in this thesis. Section 1.1 describes the general issue surrounding this research. Section 1.2 gives the problem statement supporting this research. Section 1.3 lists the research objectives, investigative questions, and proposed hypotheses. Section 1.4 gives the main focus of this research. Section 1.5 describes the methodology used to pursue this research. Section 1.6 lists the assumptions and limitations which affect this research. Section 1.7 describes the implications of this research.

1.1 General Issue

What does the United States Air Force (USAF) need in relation to printed electronics? Are there any applications which would be particularly well-suited to the flexible and low-cost nature of printed electronics? What can I do to advance our understanding of the area where the two previous questions overlap? The answers to these questions provide the basis for this thesis research. As printed electronics is a new and only partially understood field, the USAF needs basic research done. Chapter 2 provides current literature to explain some of the reasons behind the USAF's need to pursue printed electronic research. At the convergence of the answers to these two questions is the need to complete the basic characterization of inks used in printed electronic applications. This research will seek to further investigate the convergence mentioned above.

1.2 Problem Statement

The USAF and Department of Defense (DoD) are looking to develop methods and processes for creating printed electronic devices for a wide range of applications [1] [2]. For USAF printed electronics to become a reality, application needs must be identified and devices must be designed. Inks and substrates must be characterized and deposition methods must be devised. The first step to developing a printed electronic device is characterizing the ink with which the device will be printed. Without proper characterization, the ink's performance parameters will remain unknown, and device creation will be nearly impossible. CNTs present an interesting option for a printed electronics ink that has yet to be characterized. An electrical and physical characterization of CNT ink will improve the USAF and DoD's understanding of the entire field of printed electronics.

1.3 Research Objectives, Questions, and Hypotheses

This section presents the objectives this research is intended to meet, as well as the questions and hypotheses which will be used in meeting the research objectives.

1.3.1 Research Objectives.

The objective of this research is to provide an electrical and physical characterization of the CNT-based ink provided by [Brewer Science](#) © as it occurs in its printed state. The characterization provided by this research will describe ways in which the CNT ink can be effectively used in printed electronic applications.

1.3.2 Investigative Questions.

The questions asked in this research include: What is the resistivity of the ink? What is the conductivity of the ink? What are the S-parameters of the ink? How do the electrical characteristics of the ink depend on the deposited ink's thickness? What is the minimum and maximum thickness with which the ink can be deposited? How uniformly can the ink be deposited? What is the surface morphology of the printed ink? How accurately can the

ink be printed? How well does the ink adhere to its substrate? How does the substrate affect the adhesion properties? In what applications can this ink be effectively used? Answering the questions proposed in this section will provide a complete and useful electrical and physical characterization of the CNT ink provided by Brewer Science ©.

1.3.3 Hypotheses.

The hypotheses proposed for the previously stated research questions are formulated using the general knowledge of CNTs summarized in Chapter 2 and estimates provided from Brewer Science © [3]. The resistivity and conductivity of the ink is hypothesized to be about that of bulk CNTs or metal [4] [5]. A conductivity on the order of $10^7 S \cdot m$ can be expected. Table 1.1 provides the values of conductivities for various bulk metals and CNTs. The S-parameters for CNTs are also hypothesized to be about that of bulk CNTs.

Table 1.1: Bulk Conductivity of Metals and CNTs [4] [5]

| Metal | Bulk conductivity $S \cdot m (\cdot 10^7)$ |
|--------------|--|
| CNT | 1 |
| Copper | 5.95 |
| Silver | 6.29 |
| Aluminum | 3.77 |
| Tungsten | 1.79 |

The electrical characteristics of the CNT ink are hypothesized to become exponentially more efficient with an increase in thickness. This means that the transmission lines made with CNT ink will have improved transmission response with thickness and the RF reflectance will decrease. Figure 1.1 shows the hypothesized dependence of conductance and resistance on deposited ink thickness. The minimum and maximum thickness of

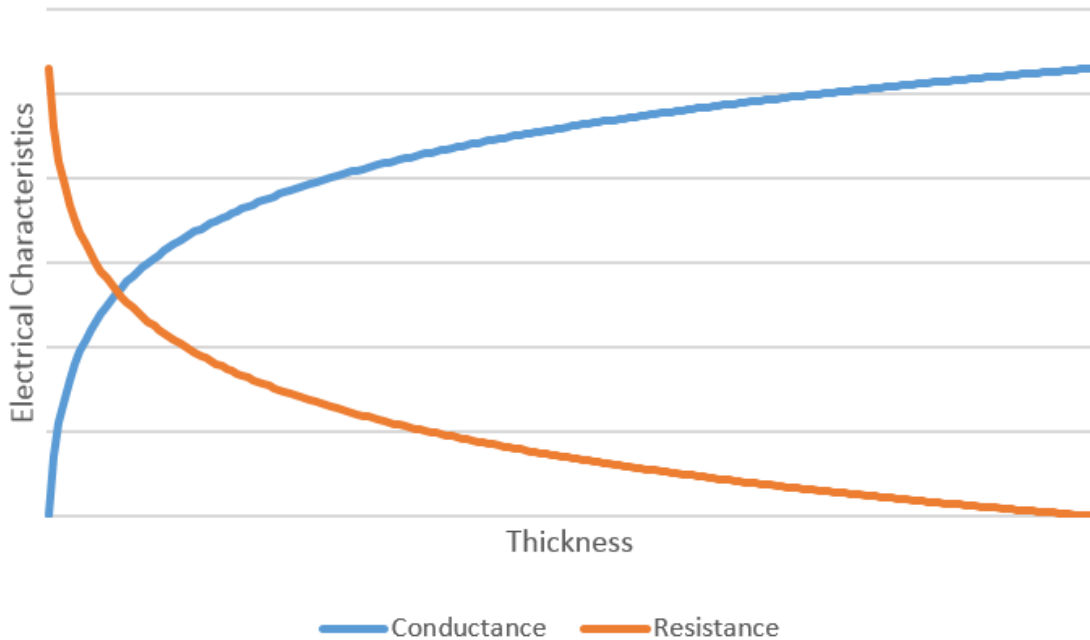


Figure 1.1: Hypothesized dependence of electrical characteristics on deposited ink thickness.

the printed ink are hypothesized to be largely dependent on the surface energy of the substrate. The reason for this is that hydrophilic substrates such as paper will result in thinner depositions, while hydrophobic substrates such as glass and polyimide will result in thicker depositions. The ability to print ink to have a specific morphology, uniformity and accuracy is hypothesized to be mostly due to the surface energy of the substrate. Substrates with higher surface energies are hypothesized to produce less accuracy and uniformity, due to the tendency of a liquid to form low contact angles with high energy surfaces [6]. The ink is hypothesized to adhere to all substrates well enough to pass the tests that will be described in Chapter 3. Based on the hypothesized results given in this section, the CNT ink is hypothesized to be useful in the creation of CNT conductive lines, simple components such as capacitors, inductors or resistors and thin film transistor (TFT)s.

1.4 Research Focus

The primary focus of the research contained in this thesis is the electrical and physical characterization of CNT-based ink. The research focus investigates the CNT-based ink as well as device design, construction, and analysis. Successful results are defined as data that allows the uses and applications for the ink to be determined. Research results will be deemed not successful if a complete characterization of the ink is not documented.

1.5 Methodology

The methodology used to answer the research questions is described thoroughly in Chapter 3. A preliminary methodology is implemented to test and calibrate the printer and test equipment. This provides data on the functional use of design and test equipment for future research and the implementation of printed electronics applications. A primary methodology is used to print and test samples and gather data on the electrical and physical characteristics of the printed ink. This provides the USAF and commercial world with data on the properties of the CNT-based ink and its uses.

1.6 Assumptions and Limitations

The primary assumption in this research is that future use of the CNT-based ink will be done under laboratory conditions similar to those under which this research has been completed. If this assumption is disregarded, the characterization this research provides may prove to be inaccurate due to the introduction of outside contaminants, stress, and forces. The most significant limitation in this research is the time required to deposit ink with the printer. The time required, along with the small working area of the printer, limit the speed of production. Due to this limitation, devices and test subjects will be carefully designed and implemented. The CNT-based ink is produced by Brewer Science ©. Therefore, its composition cannot be significantly altered by the researchers. This limits

our ability to modify the ink in reaction to the results of testing. The ink used in this research is not commercial grade, and is not sold to the general public.

1.7 Significance

This research provides a complete electrical and physical characterization of the Brewer Science CNT ink. This characterization allows future use of the ink to be streamlined, accurate, and effective. Well-defined parameters allow future users to implement the ink in their own designs with minimal testing and characterization. The primary implication of this fact is that the USAF and DoD have another well-characterized ink to add to their tool set of printed electronics materials.

II. Literature Review

2.1 Chapter Overview

This chapter reviews and discusses the pertinent and preeminent literature applicable to this project. Section 2.2 provides a description of the literature discussion in Chapter 2. Section 2.3 discusses the body of the literature review. Sections 2.3.1 through 2.3.5 present background information on CNTs and the current uses of CNTs in leading research. Section 2.3.6 presents information on leading research with CNTs derived from graphene. Section 2.3.7 discusses research conducted on printed electronic circuits. Section 2.3.8 presents research conducted by the PrinTronics Laboratory at Air Force Research Laboratory (AFRL). Section 2.3.9 presents research concerning the feasibility of printed RFID circuits. Section 2.3.10 discusses various inkjet printing techniques used in the fabrication of printed electronic circuits. Section 2.3.11 discusses the manner in which the aerosol jet printer deposits ink. Section 2.4 gives the summary of Chapter 2.

2.2 Description

The early sections of this literature review - Sections 2.3.6 and prior sections - are concerned with CNTs. The aspects discussed are the physical properties of CNTs, methods for producing CNTs, and current applications in which CNTs are being used. The current applications discussed use CNTs bonded with various substrates, although the deposition method for the CNTs may or may not be printing. The later sections of this chapter - Sections 2.3.7 and after - are concerned with printed electronics. The aspects discussed are the methodology, results, and current applications in which printed electronics are being used. The current printed applications discussed pertain to the general technique and the use of printed electronics with any ink, unless a specific ink is mentioned. This literature review in its entirety represents a thorough study of the background knowledge which

supports the field of printed electronics and the specific task of characterizing a printed ink's electrical and physical properties.

2.3 Relevant Research

The field of printed electronics in general, and especially the area concerning CNT based circuitry, is of current and future use to the USAF and DoD. The USAF has awarded contracts to companies that specialize in printed electronics [1]. AFRL contracted Optomec to create aerosol jet printers capable of producing CNT based TFTs [1]. These TFTs will be useful in wearable, flexible sensors used to integrate pilots with their aircraft and to connect them to active health monitoring systems [7]. To this end, the USAF has established the Nano Bio Manufacturing Consortium (NBMC) to contract and develop wearable sensor technologies [2]. These biological sensors are produced by depositing microfluidic inks via printers. The following research is relevant for the following reasons. First, it may relate directly to the characterization of CNT inks. Second, it may relate to the nature, characteristics, and/or production of CNTs. Third, it may relate to the possible applications of printed CNT-based circuits and their integration into the world of Very Large Scale Integration (VLSI).

2.3.1 *Carbon Nanotube Background.*

CNTs are an allotrope of carbon which use carbon rings to form a cylindrical nanostructure [8]. This is done by creating a one-atom thick sheet of graphene, which is then chemically rolled to produce a single or multi-walled CNT [9]. CNTs can be used to increase the strength of lightweight materials, as they have high tensile strength. SWCNTs have been shown to have tensile strengths as high as 22.2 GPa [10]. Some CNTs can be used as semiconductors while others can be used as metals [11].

2.3.1.1 *Electrical, Thermal, and Optical Characteristics of Carbon Nanotubes.*

The theoretical maximum electrical conductance of a single SWCNT is $2G_0$, where G_0 represents the conductance quantum which is equal to $7.748\,09 \times 10^{-5}$ S [12]. The

theoretical maximum current density of a single SWCNT is 4×10^9 A· cm⁻², which is 1,000 times greater than most metals [13]. The thermal conductivity of SWCNTs at 22 °C has been shown to be 3500 W·m⁻¹·K⁻¹ along the axis of the CNT [14]. This is roughly ten times as thermally conductive as copper, and 2,000 times as conductive as a SWCNT across its axis. CNTs have an optical absorption of 0.98-0.99 in the ultraviolet, visible, and infrared wavelengths [15]. CNT's absorption approaches that of a black body.

2.3.1.2 Structure of Carbon Nanotubes.

Whether a particular nanotube behaves as a metallic or semiconducting material can be determined based on its structure [11]. The structure of a CNT is represented by a pair of numbers, (n_1, n_2) , which is called the chiral vector [16]. These numbers represent points on a plane of graphene, with $(0, 0)$ representing an arbitrary carbon atom in the graphene plane. Each number in the pair represents another carbon atom, with n_1 representing a horizontal coordinate, and n_2 representing a vertical coordinate. For example, $(10, 5)$ would be the carbon atom ten atoms to the right of the arbitrary atom, and five atoms down from the arbitrary atom. The line from the arbitrary atom to the (n_1, n_2) atom represents one side of the graphene sheet that is to be rolled up to create the equivalent CNT. If $2n_1 + n_2$ is a multiple of 3, then the CNT which (n_1, n_2) represents is metallic.

2.3.2 Cooling.

As typical silicon-based processors become increasingly dense, methods must be found to dissipate the constantly increasing amount of heat they generate. Currently, vertical paths between layers of circuitry - known as “vias” - conduct the heat generated by individual transistors to the surface area of the chip’s package. This heat can then be transferred to a heat sink, air, or liquid cooling system. The efficiency of the entire cooling system, however, is limited to the efficiency of the vias. If the vias are poor conductors of heat, the chip will continue to heat up, which may cause device failure. For this reason, more efficient cooling methods are always important to research. The Department of

Energy (DoE)'s Lawrence Berkeley National Laboratory (LBNL) has developed a method of cooling involving carbon nanotubes using previously unexplored technology, which is described in their paper titled, "Enhanced Thermal Transport at Covalently Functionalized Carbon Nanotube Array Interfaces" [17] and in this paper in Sections 2.3.2.1 and 2.3.2.2.

2.3.2.1 Methodology.

Frank Ogletree, of Berkeley Lab's Materials Sciences Division (MSD), uses organic molecules to bind CNTs to metallic surfaces through covalent bonds. This type of stronger bond allows the CNTs to dissipate six times as much heat as when used with previous methods [17]. Additionally, Ogletree's technique is executed with gas vapors and liquids at temperatures less than 450 °C, making it compatible with current silicon-based architecture processes. The MSD's new method works for oxidizing metals such as aluminum and silicon, as well as noble metals such as gold and copper, further increasing its compatibility with modern microprocessor designs. For oxide-forming metals, aminopropyl-trialkoxy-silane (APS) is used, while cysteamine is utilized for copper and gold. In the test described in the paper, CNTs are grown on silicon wafers, then the open ends are bonded with a metal film. The bond is strong enough that the CNTs can be pulled free from the silicon substrate [17]. These bonding methods present novel materials for the printed electronics field for adhering ink to metallic surfaces.

2.3.2.2 Utilization.

While this technology still has technical hurdles to remove before mass commercial manufacturing becomes possible, its applications are readily visible. For instance, the bonds that formed between the CNTs and metal film are much stronger than before, even though some of them fail to adhere, thus reducing the density of the CNT array. However, Berkeley Lab's MSD has teamed with researchers at Intel Corporation to increase the ratio of successful bonds to breaks [17]. Second, this method of creating CNT cooling arrays has only been tested on films of metal which had been evaporated onto a glass slide. While

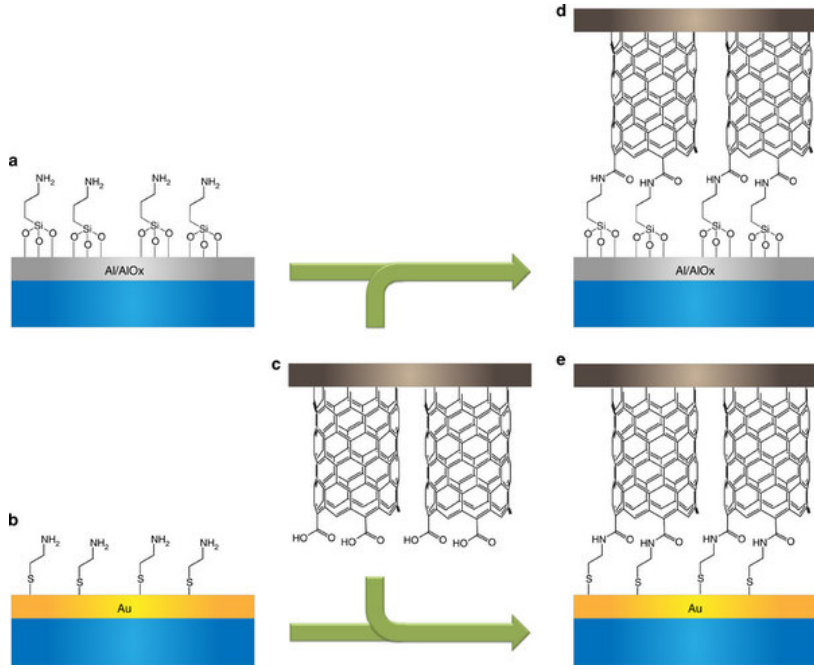


Figure 2.1: Bonding schemes for noble and oxidizing metals [17]

this is very similar to the construction of parts of a silicon-based microprocessor - thin layers of metal over silicon oxide - it needs to be tested and refined extensively. If this technology of CNT bonding can be perfected, it could lead to more efficient heat dissipation in multilayer electronic devices, chipping away at one of the preeminent problems in current day computer architecture.

2.3.3 Dense CNT Arrays.

A primary problem faced by proponents of CNT-based cooling applications for microprocessors is the relative inability to grow high density CNT “forests” that are arrays of tightly-packed parallel carbon nanotubes. These arrays need to be vertical and parallel to each other to increase their density. Researchers at Cambridge University in England have found a way to manufacture this type of structure [18].

2.3.3.1 Methodology.

John Robertson, a professor of electronic devices and materials at the University of Cambridge (UK), grew CNTs on titanium-coated copper supports which had been coated with cobalt and molybdenum. These catalysts enabled Robertson and his colleagues to construct dense CNT arrays at 450 °C, which is a temperature low enough to be process friendly in the semiconductor industry. These arrays proved to be five times more dense than any other known method, as of September, 2013 [18]. The analysis of the scanning electron microscope output produces Figure 2.2, with the results of Robertson's new method depicted on the right hand side of the figure. Robertson's article, "Low

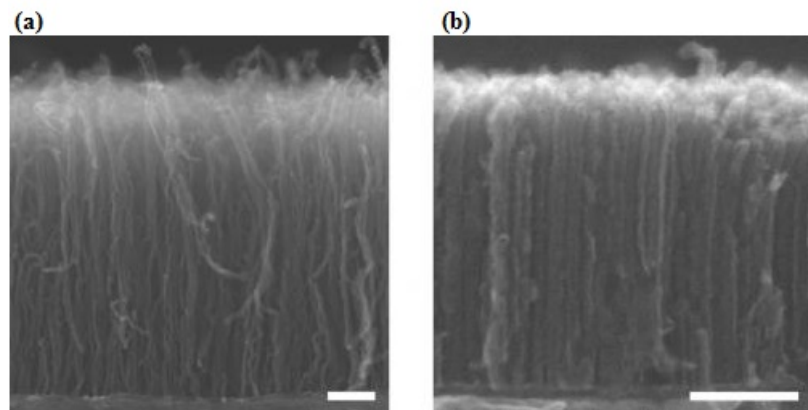


Figure 2.2: CNT arrays. (a) shows a forest of CNTs. (b) shows a forest of CNTs grown using Robertson's method. [18]

temperature growth of ultra-high mass density carbon nanotube forests on conductive supports," appeared in the August 2013 issue of *Applied Physics Letters* [18].

2.3.3.2 Utilization.

High density CNT arrays could be utilized in the design of electronic interconnects, thereby speeding up the transmission speed of signals in a silicon-based architecture. CNT

interconnects have been shown to outperform copper wires at local, intermediate, and global levels [19]. The ability to create this structure would reduce the delay caused by wires and interconnects, drastically reducing the effect of skew on design and architecture. Increased transmission speeds could also be used to increase the clock speed, and thus the performance, of a microprocessor. However, in his article, Robertson cites the CNT forests' average height as $0.38 \mu m$. At this length, CNTs would have to be combined for any sizable distance, leading to further design complications such as the difficulty of aligning and connecting millions of CNTs to provide an electrically conductive medium. CNTs could be haphazardly placed - a method which would be much faster than alignment and connection - but this arrangement would significantly reduce the conductivity of the CNTs, the very property for which they are selected.

2.3.4 Sensing.

CNTs can be used to enhance the sensitivity of certain types of sensors, as well as to decrease their size. These CNT sensors are small, versatile, and easily manufactured.

2.3.4.1 Methodology.

Ali Javey, of the Berkeley Lab's MSD, coated high-aspect ratio elastic fibers with conductive CNTs to produce electronic whiskers, or e-whiskers. This was achieved using a CNT-based paste that solidifies into a conductive and pliable composite. The composite was endowed with silver particles to increase its mechanical sensitivity, and then painted onto elastic fibers [20]. Figure 2.3 shows the production process used by Javey's team

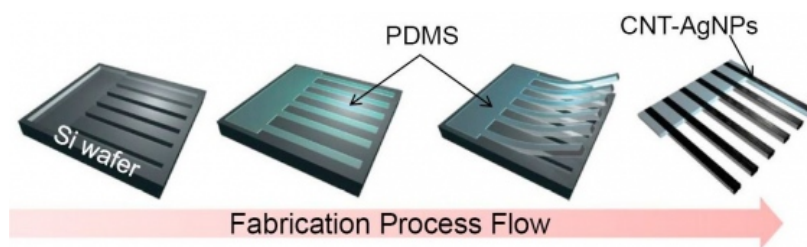


Figure 2.3: e-Whisker production diagram [20]

to develop the e-whiskers. Polydimethylsiloxane (PDMS) is the substrate used to hold the CNT-silver paste. Javey's findings can be found in greater detail in his paper, "Highly sensitive electronic whiskers based on patterned carbon nanotube and silver nanoparticle composite films," published in *Proceedings of the National Academy of Sciences* [20].

2.3.4.2 Utilization.

E-whiskers have an extremely low spring constant, allowing them to sense changes in air pressure on the order of 1 Pa. This sensitivity is roughly ten times greater than that of capacitive and resistive pressure sensors currently in production. Combined with their small sizes, this lends them to applications in robotic sensing and medical instrumentation. Javey and his team have used them to construct two and three dimensional maps of wind flow [20]. Figure 2.4(a) and Fig. 2.4(b) show the placement positions of seven e-whiskers

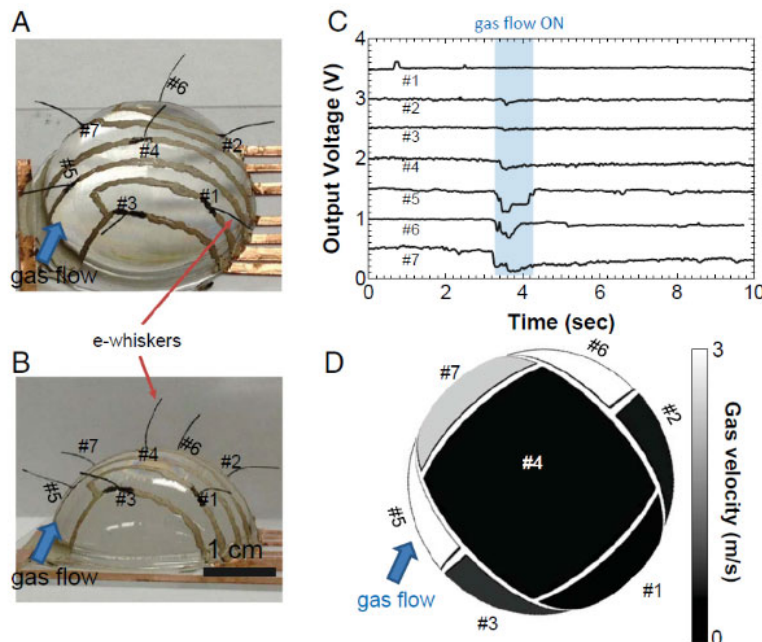


Figure 2.4: e-Whisker utilization diagram [20]

on a hemisphere of rigid plastic. Fig. 2.4(c) and Fig. 2.4(d) show how the e-whiskers respond to a change in air pressure caused by a gas flow being induced.

2.3.5 Photoreaction.

CNTs efficiently convert light into heat. As previously discussed, they are also extremely efficient in the realm of heat flow. A combination of these two effects, along with materials which are sensitive to heat, permits the creation of very precise light sensors [21].

2.3.5.1 Methodology.

Ali Javey, mentioned above, bonded arrays of SWCNT to highly pliable plastic. SWCNTs with varying chirality distributions were utilized, thus creating a sensor that responded to a specific wavelength of light. As photons strike the forest of SWCNTs, they are converted to heat which is efficiently transferred to the polymer substrate. As the polymer substrate absorbs heat, it warps in a way that can be predetermined or structured [21].

2.3.5.2 Utilization.

Javey and his team oriented the photoreactive sensor so the substrate layer contacted a larger stretch of fabric-like material. When exposed to light, this material then folded up in a manner consistent with opening curtains. This led Javey's team to suggest a future use of this technology in automatic curtains. A more practical application would be in robotic sensing, as the sensors Javey developed work well in low light levels. They are simultaneously fast and wavelength-selective, properties that up until now were deemed exclusive. For example, at room temperature the sensor bent 90° in 0.50 s. The peak absorption wavelengths of the CNTs used were 560 nm and 970 nm. Another practical application of these photoreactive CNT sensors would be in light-driven nanomotors. A circular ring of Javey's light-sensitive material would warp when exposed to light, altering the center of gravity of the ring, causing it to rotate and warp again. This motion would continue as long as a source of light was present [21].

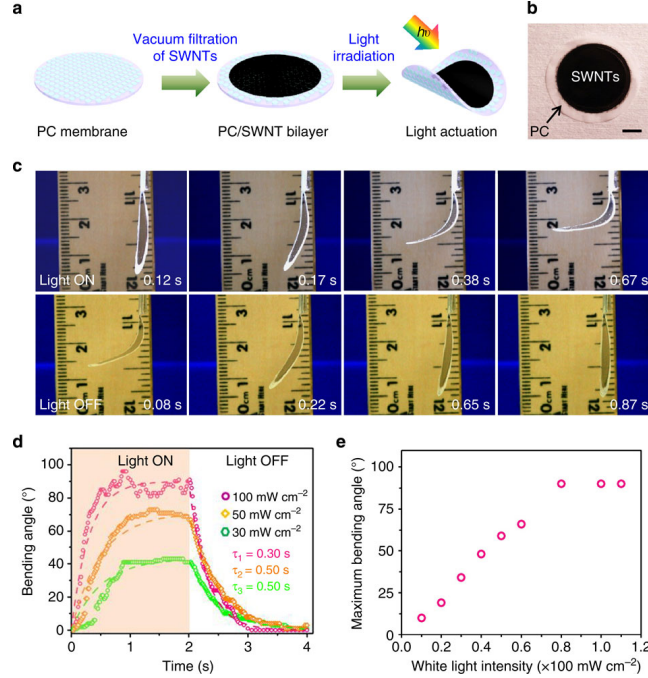


Figure 2.5: SWCNT photoreactor utilization diagram. 2.5(a) shows construction and actuation of a SWCNT photoreactor; 2.5(b) shows a photograph of a SWCNT photoreactor; 2.5(c) shows time lapse photographs of a bending SWCNT photoreactor; 2.5(d) shows bending angle as a function of time for multiple wavelengths of light; 2.5(e) shows maximum bending angle as a function of white light intensity [21].

2.3.6 Semiconductors.

Graphene has long been known to be a semiconductor under the right conditions. However, methods for producing graphene sheets of reliable size and shape have been scant. Researchers at Rice University and Stanford University have found a way to create graphene ribbons from CNTs using chemical etching and manipulation [22], [23].

2.3.6.1 Methodology.

Hongjie Dai, of Stanford University, utilized a technique known as “unzipping” to create rectangular graphene ribbons that were 10 nm wide. This achievement was done by placing CNTs on a polymer film and then etching them with ionized argon gas. This

causes the CNTs to unzip, creating a uniform sheet of graphene [22]. Another group at Rice University has used chemicals to unzip graphene sheets; however, this produces larger ribbons (of the order of 100-500 nm). Dai's article, "Narrow graphene nanoribbons from carbon nanotubes," was published in *Nature* in 2010. Since then, researchers in Finland and Sweden have encapsulated graphene ribbons in single-walled CNTs, effectively creating an insulated nanowire [23]. Fig. 2.6 shows an image of a single walled nanotube wire. These nanowires are scalable and easily constructed.

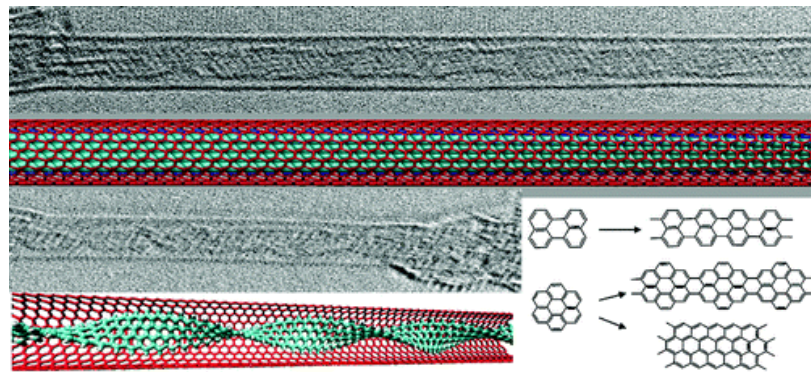


Figure 2.6: Single walled carbon nanotube encapsulating a graphene ribbon [24]

2.3.6.2 Utilization.

Dai's graphene ribbons are semiconducting, allowing them to be utilized to produce transistors. Varying the width of the graphene ribbon makes it change between acting like a metallic element and a semiconductor, depending on the number of carbon atoms across the width [24]. This is true of SWCNTs as well. Such precise control over the inherent properties of an SWCNT encapsulated ribbon would allow researchers to create nanowires, nanoantennas, *et cetera*. It is unclear as to whether these transistors are competitive with current technologies [25]. Rice University's larger ribbons are not conductive, meaning they would be confined to non-electronic uses [23]. Nanowires could be used in creating very small antennas or wires inside a processor. However, uses for non-

conductive nanoribbons are limited to mechanical, structural, and thermal applications. These include reinforcing a material and transferring heat from one material to another.

2.3.7 Printed Electronics.

Printed Organic FETs have been shown to be a viable technique for producing flexible printed circuitry, with an entire range of electronics being built based on organic printed n-Type Field Effect Transistor (NFET)s and p-Type Field Effect Transistor (PFET)s. Some researchers have even managed to combine printed electronics with structural components to create 3D functional printed electronic devices [26].

2.3.7.1 Printed Organic FETs.

G. L. Whiting, *et al.* describe in their paper, “Printed circuits and sensing systems”, methods they have created for producing circuits based entirely on printed organic FETs [27]. These circuits are constructed using ink jet printing methods in a low-temperature (450°C), process-friendly environment. Complementary logic circuits, power sources, and sensors were all printed and combined in a single large-area circuit. Separately printed, flexible batteries were also designed, printed and characterized. Whiting and his team extracted design rules and models from the printed circuits to simulate and study the effects of process variation in ink jet printed circuits [27]. Figure 2.7 shows a temperature sensor printed by Whiting and his team. The sensor has a simple screen and configurable, rewritable memory. It is printed on a flexible plastic substrate. Many applications for

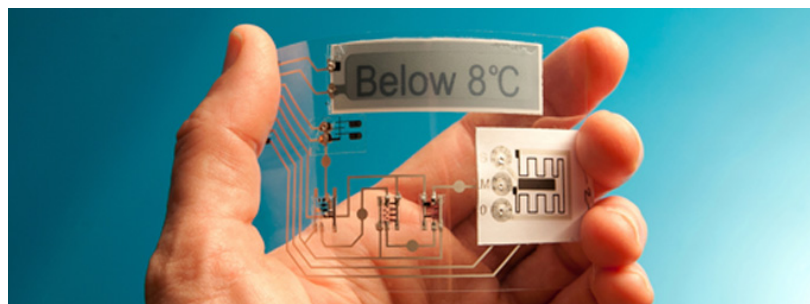


Figure 2.7: Printed temperature sensor with rewritable memory and screen [27]

flexible, printed, self-contained circuits exist in the modern day world. Health monitors, item-level tracking, and durable electronics are just a few that are of interest to the USAF.

2.3.7.2 Electronic and Structural Printer.

PARC, owned by the XEROX Company, has been investigating 3D printers which could possibly combine the structural and electronic aspects of traditional devices into a single functionality. In a sponsored paper published in October of 2013 titled “3D printed electronics”, Steven Ready, *et al.* describe a combined printer they have constructed which has the capability of printing both electronic and structural details on the same medium, from the same device, in a single run [26]. The purpose for developing such a printer was to “provide means of manufacturing functional objects which may be difficult to manufacture or even not be manufacturable by other means,” by integrating structural materials with functional electronic mediums [26]. By incorporating extrusion techniques for laying

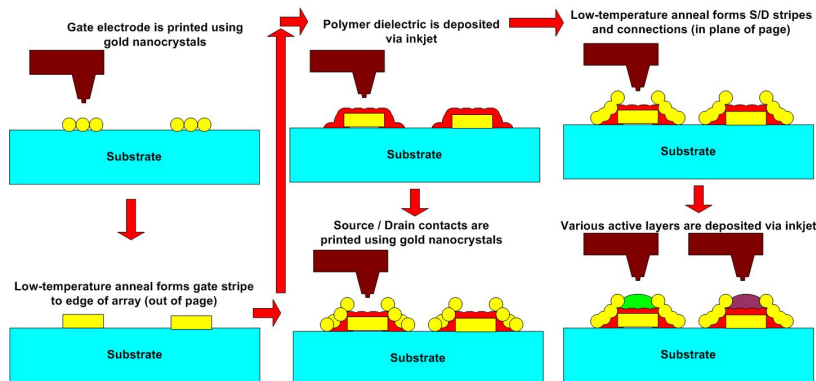


Figure 2.8: Ink jet process for printing a flexible FET [26]

structural materials and ink jet techniques for printing electronic mediums, the PARC team was able to construct a printer which could handle inks with a wide range of viscosities. Their printer is also capable of patterning inks into smooth features as small as tens of microns across [26]. Figure 2.8 shows a diagram of how the PARC printer constructs a flexible FET.

2.3.8 Printronics Laboratory Research.

The following research has been generated by the Printronics Laboratory at AFRL. The Printronics Laboratory sponsored my thesis work. The Printronics Laboratory provided laboratory space, the Dimatix and Optomec printers, a profilometer, clean room space, Scanning Electron Microscope (SEM) equipment and operation, and a network analyzer.

2.3.8.1 Printed Photodetectors on Paper Substrates.

In a Printronics paper published 1 February 2014 titled “Performance of a Printed Photodetector on a Paper Substrate”, Aga, *et al.* describe the performance of a photodetector printed in-house on HP photo paper with five different inks [28]. P3HT:PCBM is utilized as the photoreactive layer printed on top of a silver electrode. PEDOT:PSS was used as an interface between the P3HT:PCBM and silver electrode to aid in adherence between the two layers. A layer of DNA biopolymer was drop cast on top of the P3HT:PCBM to create a neutral surface with which the PEDOT:PSS could bond. Without the crucial DNA interlayer, the PEDOT:PSS bubbled up and formed an non-uniform top electrode [28]. In Figure 2.9, we can see the effects of the DNA interlayer on the PEDOT:PSS/P3HT:PCBM bond. Figure 2.10 depicts the various responses of Aga *et al.*’s photodetector. Note that the photodetector was responsive to all tested wavelengths between 405 nm and 635 nm, with 405 nm producing the best response [28]. Due to the high conductivity of the DNA biopolymer, a large current is passed when the photodetector is not excited. All information in section 2.3.8.1 was gathered from the paper named above. [28]

2.3.8.2 Biotronics and Salmon Waste as Ink.

Biotronics is a relatively new research area that uses biological materials to construct electronic devices [29]. One new application that was utilized in the photodetector discussed in subsubsection 2.3.8.1 is DNA as a conductive, optically clear material. This

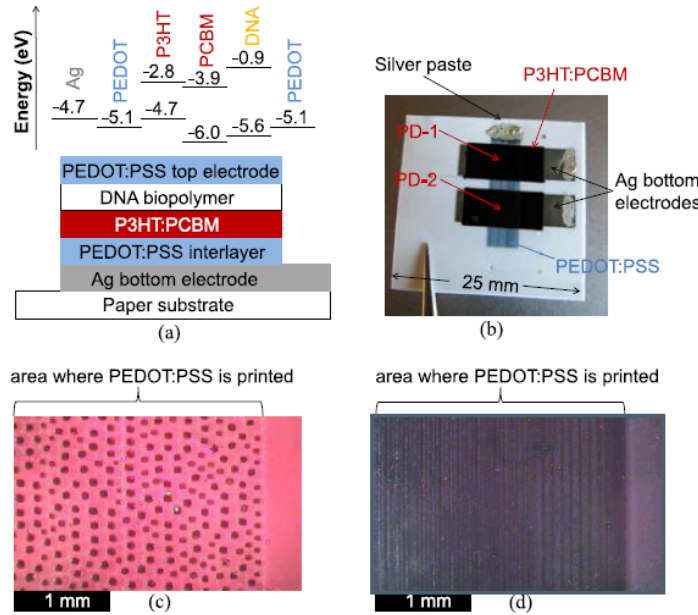


Figure 2.9: Photodetector device cross-subsection with material energy levels (a); two PDs on paper substrate (b); PEDOT:PSS when printed directly on P3HT:PCBM (c); PEDOT:PSS on P3HT:PCBM with a DNA interlayer (d) [28].

DNA biopolymer is created by obtaining DNA from salmon milt and roe, and then precipitating it with hexadecyltrimethylammonium chloride (CTMA) to create a white crystalline powder that is soluble in organic solvents. This powder can then be mixed with water to create an ink solution usable in ink jet and aerosol jet printers [29]. For more information on this process, see "Biotronics for Defense" by Heckman published in SPIE Professional in April 2011. All information from subsubsection 2.3.8.2 was gathered from the paper mentioned.

2.3.8.3 Bio-Organic FETs.

An international team of researchers from Austria, Australia and Turkey have worked with Dr. Carrie Bartsch, Dr. Jim Grote and Dr. Josh Hagen at AFRL to show that transistors can be printed on a glass substrate using gold, DNA and CTMA [30]. These

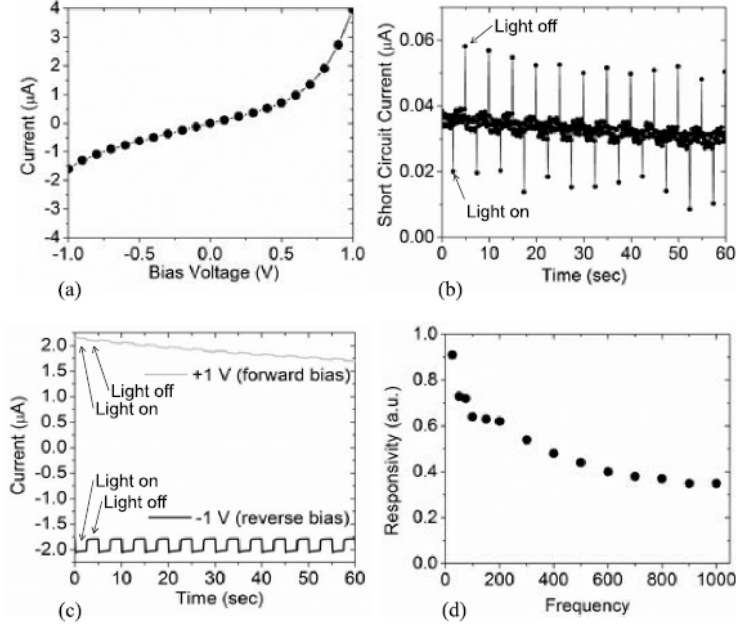


Figure 2.10: I-V characteristics of the photodetector in the dark (a); photodetector response to light pulses (b); photodetector response to light pulses under applied voltage (c); photodetector response frequency dependence at 525 nm wavelength [28].

devices have been termed bioFETs, a combination of the terms “Bio-organic,” and “FET.” While bioFETs do not function with the same performance characteristics of state-of-the-art transistors, they do show potential for being developed into faster, more reliable devices [31], [30]. Figure 2.11 and Figure 2.12 shows the layout and performance characteristics of the this bioFET. One design hurdle experienced by the team was the DNA-CTMA layer failing to bond. Their proposed solution was to crosslink the two materials using another, more complex bonding chemical [30]. As seen in Figure 2.11(c) and Figure 2.12(c), this improves the transfer characteristics of the bioFET, making them symmetric. This research team was able to construct both n-type and p-type bioFETs.

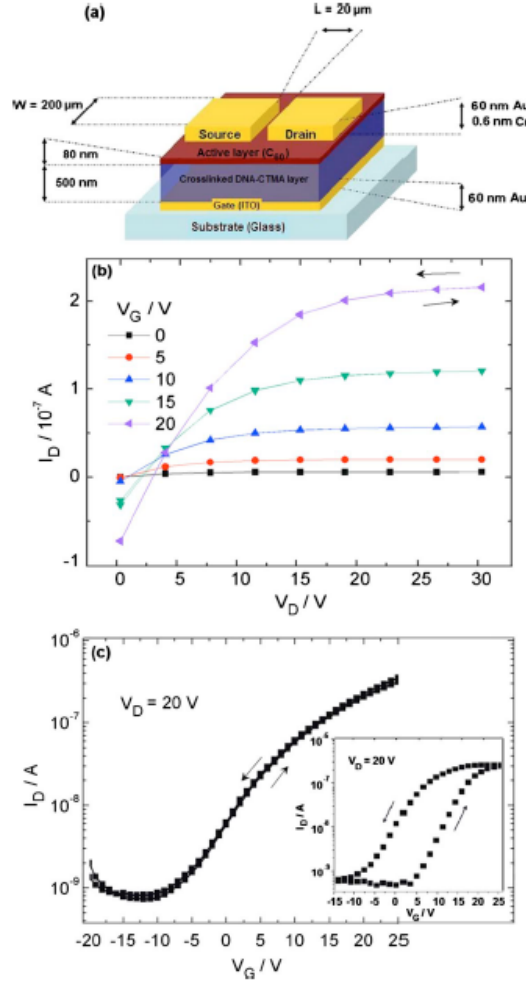


Figure 2.11: Performance of a DNA-based bioFET. 2.11(a) shows the layout of an n-type bioFET device; 2.11(b) shows the output characteristics of an n-type DNA-based bioFET device; 2.11(c) shows an n-type bioFET's transfer characteristics for the given voltage; 2.11(c) inset shows an n-type bioFET's transfer characteristics for the given voltage when non-crosslinked DNA is used [30].

2.3.9 Feasibility of Printed RFID Circuits.

This section discusses research in printed RFID circuits. One idea generated jointly by Major DeppenSmith, Dr. Lanzerotti, and myself is the application of a printed radio-

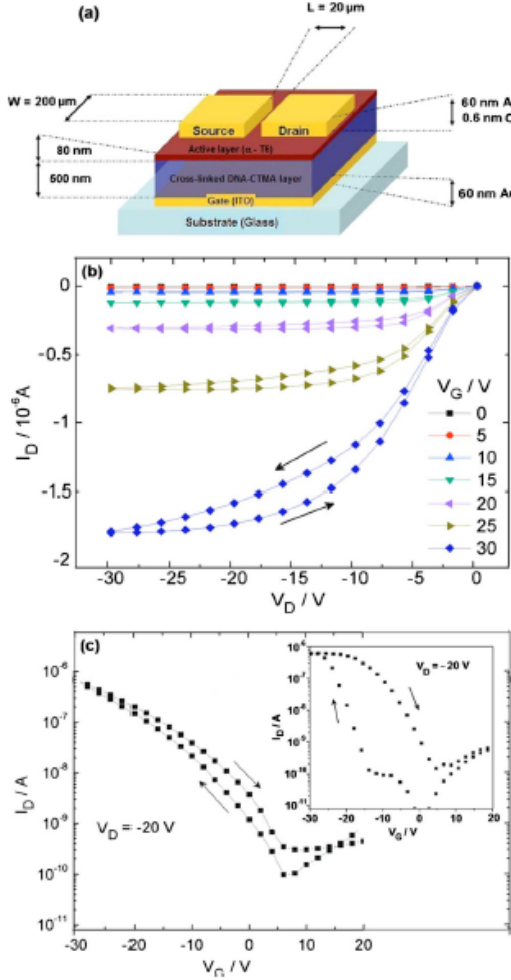


Figure 2.12: Performance of a DNA-based bioFET. 2.12(a) shows the layout of a p-type bioFET device; 2.12(b) shows the output characteristics of a p-type DNA-based bioFET device; 2.12(c) shows a p-type bioFET's transfer characteristics for the given voltage; 2.12(c) inset shows a p-type bioFET's transfer characteristics for the given voltage when non-crosslinked DNA is used [30].

frequency identification circuit that could be used as a low-cost, low-profile method of targeting and identification. Upon researching this topic, I found that various grades of printed RFID circuits have already been made [32].

2.3.9.1 All-Printed RFID Circuits.

Jung *et al.*, successfully demonstrated the effectiveness of a single bit printed RFID tag operating at 102.8 Hz. The tag transmitted at a frequency of 13.56 MHz. While this falls short of the 96-bit standard needed to encode useful information, it represents a broad field of possible research. Oreccini *et al.*, demonstrated that complete, battery-free active RFID circuits can be printed on paper substrates while incorporating piezoelectric energy scavengers to supply power [33]. While both of these findings represent unique advances in the field of printed RFID circuitry, there is much more research to conduct. Some printed RFID tags are currently being used in the commercial market. For instance, the Los Angeles County Metropolitan Authority uses printed, flexible RFID tags in its temporary transit cards, which are designed to be disposable [34]. These tags operate in the 13.56 MHz bandwidth, and are passive in nature. This means that they do not use a battery, and they cannot broadcast their information. They only react to electromagnetic fields. Figure 2.13 shows a printed, flexible RFID circuit.

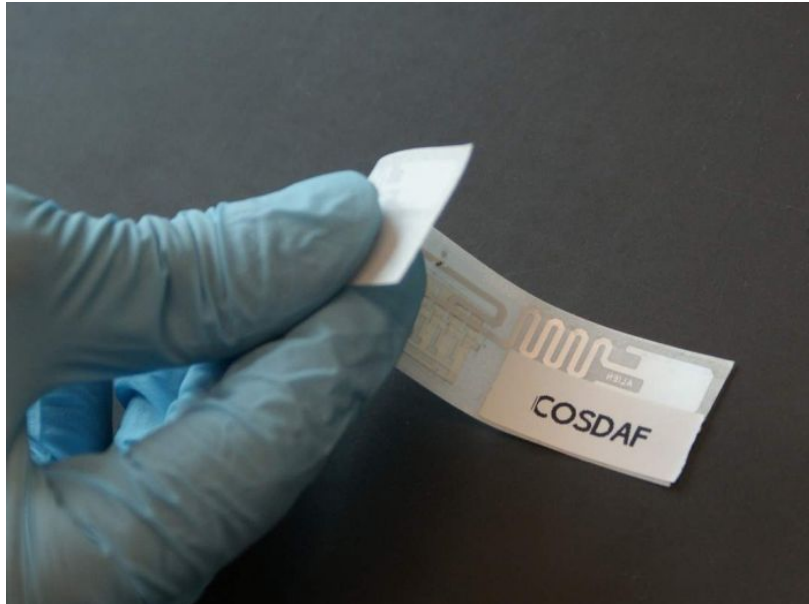


Figure 2.13: A printed RFID tag on flexible substrate [35].

2.3.9.2 Future Research.

Current research suggests that novel printed RFID tags can only transmit across a very short range - that is, distances of a few meters under laboratory conditions. This would suggest a possible research topic of characterizing and improving the compact, printed antenna on various organic and inorganic substrates. This would allow future research to be conducted into the feasibility of low-cost, roll-to-roll printed RFID tags, as well as the actual transmission distance of said tags. Another area of possible research is the effect of various inks and substrates on the performance of printed RFID tags.

2.3.10 Inkjet Printing Techniques.

This section covers research concerning basic inkjet printing techniques. CNT-based inks present an attractive solution for printed electronics in that they can be highly-conductive and can be incorporated into a thin, electrically conductive, optically clear coating called a Transparent Conductive Film (TCF) [36]. A CNT TCF can be produced using inkjet printers and techniques in a single production step, whereas other methods of production such as spray-coating and filtering require multiple “etch and mask”-like steps. Applications for an easily-produced CNT TCFs include flexible display components, optically permeable electronics, and photo-sensitive components.

2.3.10.1 Factors Which Affect Inkjet Printing.

Factors produced by the inkjet printer, print head, and piezoelectric actuators have a significant effect on the quality and accuracy of the design being printed [37]. These factors affect the manner and condition in which the ink leaves the printer and is deposited on the substrate. As a whole, the determining factors and condition of the ink is known as the “jetting condition” of the ink. Improper or uncalibrated actuation can produce satellite droplets which reduce accuracy by increasing splatter [37]. Decreased actuator voltage or above-average ink viscosity can prevent drops from fully forming, and therefore clogging the jetting nozzles [37]. Factors such as air temperature, substrate temperature,

drop speed and shape, and head angle can adversely impact design [37]. These factors can be arbitrarily assigned by altering the printing specifications. The substrate type is another factor that can be selected. Figure 2.14 shows the difference between glass and plasma-treated glass in regards to a single ink drop [36]. The plasma-treated glass not only shows better contact angle at 11° versus 54° on bare glass - but it also shows a more evenly dispersed drying pattern. The lower contact angle allows for less ink to be used to cover a certain area, while also decreasing the drying time required. The faster drying time allows the center to dry at the same rate as the edges, which keeps the CNTs from conglomerating in one section of the drop. Another controllable factor which can reduce

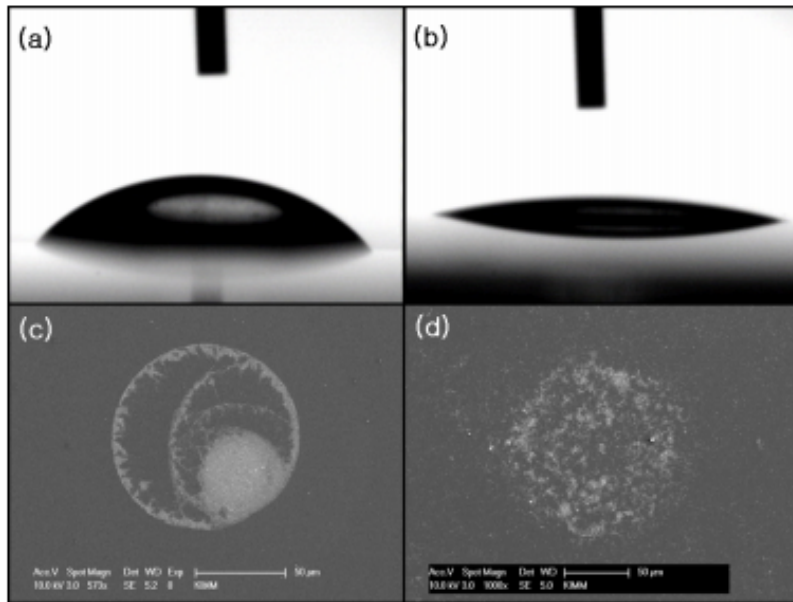


Figure 2.14: Substrate treatment effects on contact angle and CNT dispersion. (a) shows drop contact angle on glass; (b) shows drop contact angle on treated glass; (c) and (d) show drops (a) and (b) after drying [36].

drying time and affect dispersion is substrate temperature. When heated to 60°C , glass substrates showed drastically reduced drying times - from 12 s to 1.6 s [36]. This causes

the edges of ink drops to dry fast enough to allow the drop to maintain its shape. If the edges did not dry in this manner, the drop would expand, decreasing the accuracy with which shapes can be printed. Low drying times also allow multiple passes to be made on a single pattern. This can aid in printed material thickness uniformity and particulate network formation. Figure 2.15 shows the various dispersion patterns created by heated and room temperature drying of CNT ink drops. Figure 2.15 (a) shows the ringed pattern left from uneven drying rates at the center and edges of drops, while Figure 2.15 (b) shows the evenly dispersed CNTs left when the substrate is heated. However, using high heat

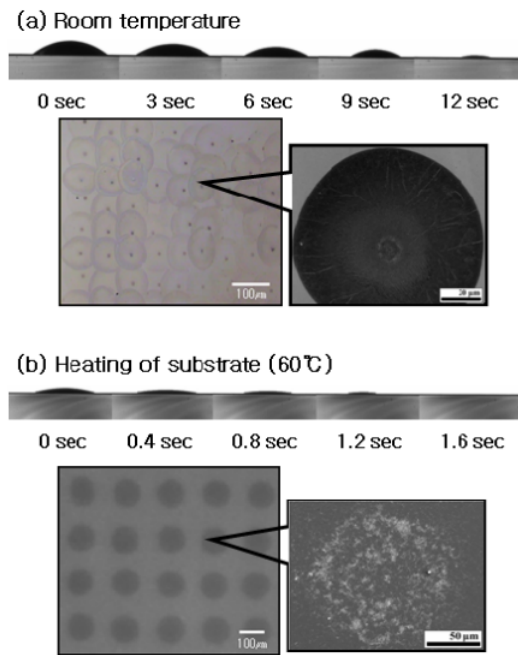


Figure 2.15: Substrate temperature effects on drying time and CNT dispersion. (a) shows CNT dispersion and drying time for room temperatures; (b) shows CNT dispersion and drying time for heated substrates [36].

to reduce drying time affects other parameters besides dispersion. Merilampi *et al.*, have shown that in the case of silver-based inks, using heat to artificially reduce drying time

will also reduce sheet resistance [38]. This is desirable because low sheet resistances in printed lines allows for higher currents to be carried. If sheet resistance was not lowered, a higher current would mean higher energy lost to heat, which would be dissipated into the substrate causing warping, burning, and/or melting depending on the type of substrate. With low sheet resistances, less power is dissipated in a design, leading to more efficient devices.

2.3.10.2 Effects of Overwriting and Line Width.

When printing CNT TCFs, two key parameters contrast each other, affecting the material's efficiency. Both the resistivity and transparency are correlated to the density, alignment, and network formation of the CNTs [36]. Resistivity is the quantification of a material's resistance to carrying a current. Generally, it can be defined by the following equation:

$$\rho = \frac{R * A}{l} \quad (2.1)$$

where the term ρ represents resistivity in ohm·meters, R represents the resistance in ohms, A represents area in square meters, and l represents length in meters.

Transparency is defined as the amount of light which is transmitted entirely through the material. Network formation is the amount that the CNTs overlap and connect with each other. Alignment is important in that CNTs are not roughly spherical, as are traditional ink particles. Rather, they have a very high aspect ratio. Because of this, if the CNTs are highly aligned - that is, parallel - few electrical connections can be made, and the printed material will have a high resistivity. The same can be said of the density of the CNTs. If the printed material has a low CNT density, resistivity will be higher than another instance of the material with a higher CNT density. Density and network formation have the opposite effect on transparency. As density and network formation increase, transparency decreases, reducing the efficiency of the TCF. Therefore, in CNT TCF applications, density must be precisely controlled so that the resistivity and transparency can be balanced. This is done

via overwriting - the process of printing the same pattern multiple times in one location so that multiple layers are put down - and changing the printed line width. Depending on the exact characteristics of the ink used - viscosity, temperature, and particulate density, for example - a single layer of printed material often does not produce the desired alignment and network formation needed for good electrical conduction [36]. However, a single overwrite provides much more network formation, while lowering resistivity. Figure 2.16 shows a Field Emission - Scanning Electron Microscope (FE-SEM) image of drop overwriting.

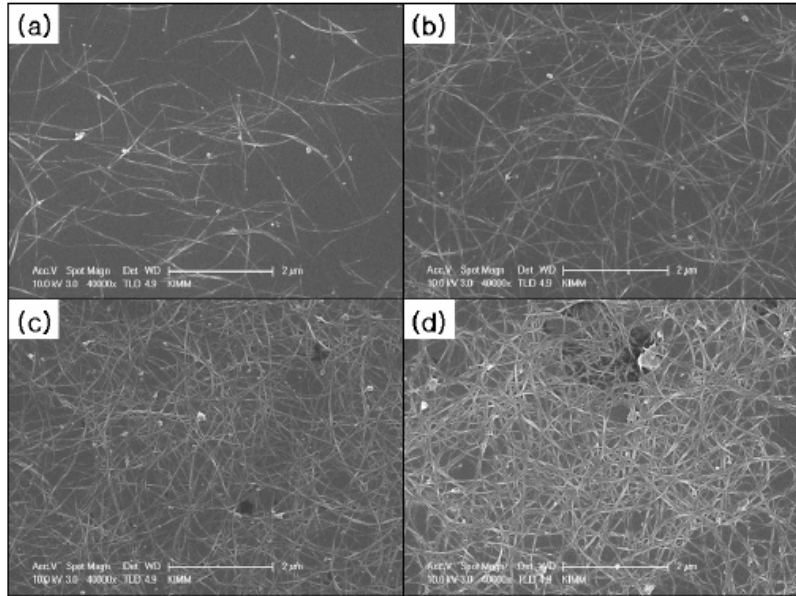


Figure 2.16: Overwriting effects on CNT network formation. (a) shows the CNT network formed after a single printed drop; (b) shows the CNT network formed after two drops; (c) shows the CNT network formed after five drops; (d) shows the CNT network formed after eight drops [36].

Figure 2.17(a) shows an image showing the effects of overwriting and line width on transparency. In the top section, the line on the far left was printed once, with each

successive line being overwritten once more than the one to its left. The line on the far right was overwritten seven times, for a total of eight layers. In the bottom section, each line is $75\ \mu\text{m}$ wider than the one to its left, and the first line is $170\ \mu\text{m}$ wide. Figure 2.17(b) shows a printed CNT circuit with 85% transparency. Figure 2.18(a) shows an image showing how increasing overwriting increases thickness while decreasing resistivity. Figure 2.18(b) shows an image showing the I-V characteristics of printed lines with increasing line widths. Song *et al.* showed that the resistance of a printed line decreases as line width increases. However, that relationship is not linear, as the resistivity of a printed CNT TCF decreases at a rate five times greater than the line width increases [36].

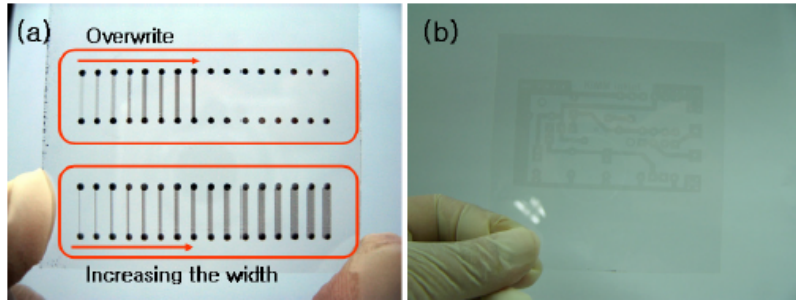


Figure 2.17: Overwriting and line width effects on CNT transparency. (a) shows the effect of overwriting and line width on transparency; (b) shows a printed CNT circuit on glass [36].

2.3.11 Aerosol Jet Printing.

The Optomec aerosol jet printer deposits a liquid ink in a different manner than the Dimatix. The ink is atomized using a mist generator, and is then collimated by a sheath gas [39]. The sheath gas carries the atomized ink through a deposition nozzle and onto the substrate. The deposited ink then dries under normal conditions, or can be subjected to

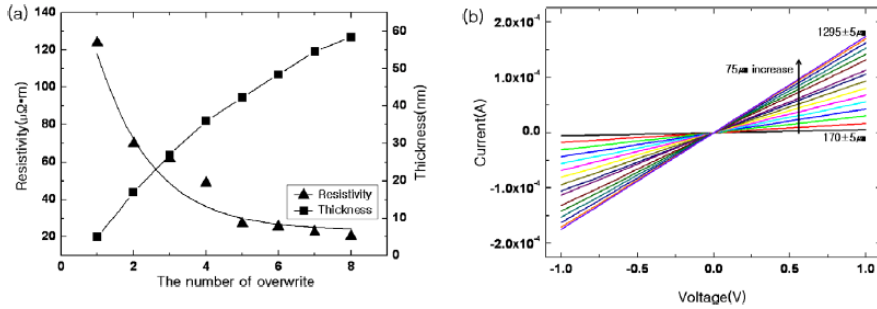


Figure 2.18: Overwriting effects on resistivity and thickness with line width effects on I-V characteristics. Fig. (a) shows the effect of overwriting on resistivity and thickness; Fig. (b) shows the I-V characteristics of printed CNT lines with varying widths [36].

heat, chemicals, or vacuum to expedite the drying process. Aerosol jet printers can create films on the order of 10 nm thick with feature sizes as small as 10 microns.

2.4 Summary

This literature review has distilled and summarized the state-of-the-art knowledge supporting the characterization of the electrical and physical properties of printed CNT ink. This chapter reviewed the properties and characteristics of CNTs, various methods for depositing CNTs, and applications in which CNTs are being used. This chapter also reviewed the method of printing electronics, organic printed circuits, printed RFID circuits, and the techniques associated with printed electronics.

III. Methodology

3.1 Chapter Overview

This chapter presents and discusses the methodology implemented during the experimentation phase of this research. Section 3.2 outlines the experimental methodology. Section 3.2.1 presents the methodology behind the initial tests. Section 3.2.2 presents the methodology behind the primary tests. Section 3.3 presents and discusses the test subjects that were constructed and utilized during testing. Section 3.4 gives a summary of Chapter 3.

3.2 Experimental Methodology

The experimental methodology is divided into an initial test section and a primary test section. The initial test section describes the methodology behind the set of tests concerning an aerosol jet ink. The primary test section describes the methodology behind the main set of tests which characterized the electrical and physical properties of printed SWCNT inkjet ink.

3.2.1 Initial Test Methodology.

Due to an insufficient supply of the needed ink, an initial test was conducted. Initial printing tests were conducted using the Dimatix DMP 2800 equipped with a DMC-11601 cartridge and Brewer Science © Aerosol Jet SWCNT ink. No circuits were printed, as the ink would not jet properly. Multiple attempts were made with various combinations of jetting waveforms and voltages, print cartridge vacuum pressures, platen and print head temperatures, nozzle purge, cleaning techniques, and jetting frequencies. In each case, all sixteen of the 9 μm printing nozzles became clogged within five minutes of the time at which the ink made contact with the print cartridge. This was likely due to a combination of factors including, but not limited to: CNT length and/or chirality, ink solvent characteristics, ink particulate suspension, and environmental variables. The

ink failed to print multiple times, no matter what the printing parameters. Because the parameters had no repeatable effect on the ability of the ink to print, the parameters are not recorded here.

3.2.1.1 Length and Chirality.

The length of the SWCNTs in the ink is unknown as the provider, Brewer Science ©, does not disclose that information. If the CNTs are too long, they could form networks in the printing nozzles, quickly clogging the entire cartridge. They could also fall out of suspension easier, clogging the nozzles and piezoelectric heads. Additionally, Brewer Science © has not disclosed the physical structure of the CNTs beyond the fact that they are single walled [40]. Various chiralities possess differing physical characteristics, some of which may be incompatible with inkjet printing, or the Dimatix DMP 2800 specifically.

3.2.1.2 Ink Solvent Characteristics.

The Brewer Science © Aerosol Jet ink consisted of SWCNTs in water. Water is a suitable solvent in some applications, but it has a relatively low drying time. This means that as the ink is moving down the lines into the printing nozzles, it has already started to dry. This can result in clogged nozzles and inconsistent jetting characteristics. To alter the solvent's drying characteristics, a thickener such as ethylene glycol can be added [40]. However, water has a high surface tension when compared to common organic solvents. This property can cause it to jet infrequently or improperly. The adverse jetting effects due to surface tension would be compounded by the use of chemicals such as ethylene glycol.

3.2.1.3 Ink Particulate Suspension.

Brewer Science © used a common suspension method with their CNT-based ink. They suspended SWCNTs in water. This type of ink is prone to clogging nozzles as any suspended particulate - particularly SWCNTs - is prone to flocculating if no surfactant is added to stop this process. Flocculation occurs when a suspended particulate clumps together and falls out of suspension. This is due to the hydrophobic nature of the outside

walls of the CNTs [41]. Water is repelled by the CNTs, leaving strong van der Waal's forces to attract CNTs to each other. Heavy clumps of particulate are then able to fall out of solution, or clog the lines and print nozzles. One method that can be utilized to overcome the van der Waal's forces present in any CNT ink is the addition of a surfactant - or amphiphilic compound with both hydrophobic and hydrophilic properties. The hydrophobic end of the surfactant bonds to the outside wall of the CNT in a process called functionalization [42]. This leaves the hydrophilic ends of the surfactants on the functionalized CNT exposed, repelling hydrophobic CNTs and attracting water molecules, thus overcoming the van der Waal's forces and aiding in particulate dispersion. See Figure 3.1 for a diagram of functionalization. The addition of surfactant to a CNT ink

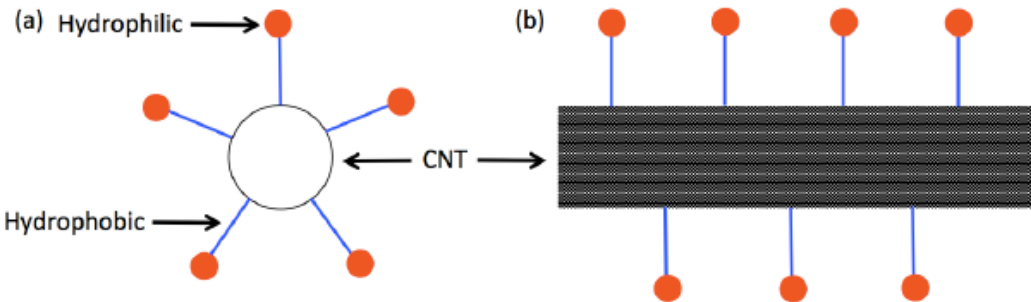


Figure 3.1: Functionalization of CNTs in solution via addition of surfactant. (a) shows a cross section of a surfactant-functionalized CNT; (b) shows the side view of the same CNT [41].

lowers the surface tension of the ink as the surfactant molecules accumulate on the interface between the ink solvent and the air [41]. This decreases the contact angle of the printed drop with respect to the substrate while increasing its diameter, thus decreasing the drying time and aiding in particulate network formation, as discussed previously. Figure 3.2 provides

an explanation of surfactant effects on surface tension. However, addition of surfactant, as well as functionalization of the CNTs can both contribute to decreased conductivity [42].

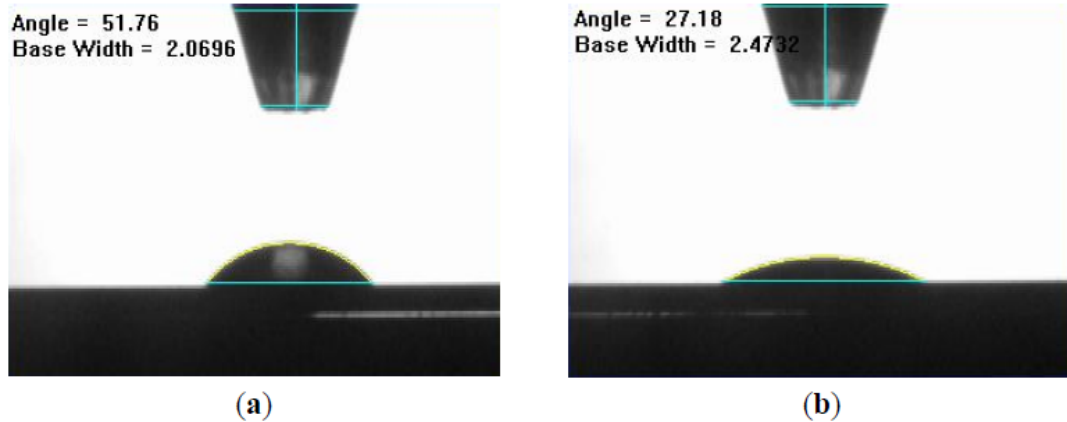


Figure 3.2: Effects of surfactant on drop surface tension. (a) shows a $3 \mu\text{L}$ drop of water on SiO_2 substrate ; (b) shows a $3 \mu\text{L}$ drop of water with surfactant on SiO_2 substrate [41].

3.2.1.4 Environmental Variables.

Variables such as air temperature and turbidity, humidity, ink temperature and viscosity, and vacuum pressure can affect the jetting characteristics of an ink. While it is likely that they played some role in the failure of the Brewer Science © ink to jet, we do not think their effects were significant, as different results were not observed in differing lab environments.

3.2.1.5 Ink Failure.

Brewer Science © provided the Printronics Lab with CNT-based inks for characterization when printed by the aerosol jet and inkjet printers. The process of inkjet printing SWCNTs was pioneered in 2007 by Small, *et al.* [43]. However, Small, *et al.* used a Commercial, Off-The-Shelf (COTS) inkjet printer, not one designed for additive manufacturing. Due to a supply shortage in inkjet ink, we tested the Brewer Science © Aerosol Jet ink

to measure its jetting characteristics in an inkjet printer. Our hypothesis prior to printing posited the ink would jet, albeit partially or inefficiently. After testing, we concluded that the ink would not jet in an inkjet printer, and that the ink destroyed the cartridges in which it was placed. Positive results have been achieved on the aerosol jet printer.

3.2.2 Primary Test Methodology.

This primary test methodology section discusses the basis and reasoning behind the tests conducted to determine the electrical and physical characteristics of printed SWCNT ink. A complete characterization of the electrical and physical characteristics of a printed ink includes parameters for resistivity and conductivity, S-parameters and modeling results of a CPW, thickness, uniformity, roll-off and sharpness of features, and adherence to and utilization of various substrates. Substrates used include COTS photography-grade paper, polyimide, and glass.

3.2.2.1 DC Test Measurements and Equipment.

Sheet resistance is determined using a four-point probe [44]. Sheet resistance can be used to calculate resistance, depending on the geometry of each sample. Resistivity can be calculated from resistance, when the exact geometry of the sample is known. Conductivity can be calculated as the inverse of resistivity. This tool consists of four equally-spaced probes in a line [45]. The outer probes force current from one to the other, causing a voltage to be applied across the material between them. This voltage is then measured by the inner probes and used to calculate the sheet resistance according to the following equation:

$$\rho_{\square} \left(\frac{\Omega}{\square} \right) = \frac{\pi}{\ln(2)} \frac{V}{I} \quad (3.1)$$

where the term V represents the voltage applied across the tested material, and the term I represents the current running through the tested material. The correction factor for the results obtained by the four-point probe is 1, and therefore does not change the measured

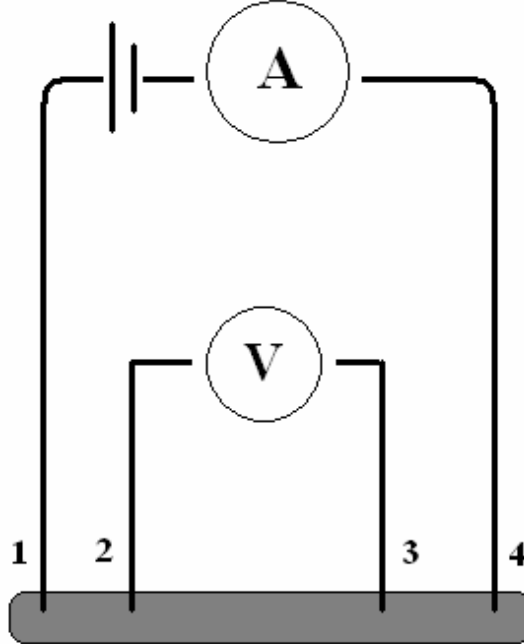


Figure 3.3: Schematic of a four-point probe. A represents the current flowing through probes 1 and 4; V represents the voltage across probes 2 and 3 [46].

results [47]. Printed samples were designed to make the applicable correction factor equal to 1.

3.2.2.2 RF Test Measurements and Equipment.

S-parameters are determined using a network analyzer. S-parameters are ratios of how much power is reflected or passed through from a port on a device [48]. Four parameters can be used to completely describe a two-port device - how much of the total applied power flows from port one to port two, how much is reflected by port one, how much power flows from port two to port one, and how much is reflected by port two. Inductance and the quality factor, Q , are measured using an LCR meter. The quality factor is the ratio of the resonant frequency, $\omega_r(r)$ to the bandwidth, B . The quality factor can be expressed using Equation 3.2 [49].

$$Q = \frac{1}{R} \sqrt{\frac{L}{C}} = \frac{\omega_r}{B} \quad (3.2)$$

In Equation 3.2, R represents resistance, L represents inductance, and C represents capacitance.

3.2.2.3 Mechanical Test Measurements and Equipment.

Uniformity and feature sharpness are determined with an electron microscope. Thickness and roll-off are determined using a profilometer. Roll-off is the amount of curve seen where the top corners should be on a printed line when the feature is viewed from the side, as in a cross-section image. This is directly related to feature sharpness and the accuracy with which a design can be printed. In printed devices, as roll-off increases, accuracy can decrease. This is due to the ink forming a half-dome on the substrate instead of forming right angles with the substrate. Adherence is determined by the tape test. The tape test is conducted by applying a flexible adhesive-backed polymer to the fully-dried printed circuit. The tape is then removed and analyzed. If a significant amount of SWCNTs are removed, the tape test fails. A significant amount of SWCNTs is defined by the amount needed to change the sheet resistance of the printed device.

3.2.2.4 Testing.

The tests involved in characterizing the Brewer Science © ink jet CNT ink proceeded in the following order. First, the cartridge, printer, and jet settings were adjusted to make the ink jet from the printer optimally and adhere properly to the chosen substrate. Then, a single dot was printed and measured to determine the minimum feature size possible. Minimum feature size was used to recalibrate the cartridge and jet settings. Lines were then printed and visually inspected. Then, the four-point probe was used to collect sheet resistance data. CPWs were printed and tested to collect S-parameter data. The SEM was then used to capture morphology and surface feature data. This data was used to adjust the design of the CPWs, which were then tested again for S-parameters. The profilometer was used to collect data on thickness. Next, the thickness data was used to adjust the design of the CPWs. The tape test was then performed to collect adhesion data. This test ordering

was conducted on paper, glass, polyimide, and Nomex © substrates. Omission of certain tests was necessary due to the physical properties of some substrates. Chapter 4 provides more information.

3.3 Test Subjects

Section 3.3 describes the printed circuits used for testing. Lines, rectangles, CPWs, and inductors were printed.

3.3.1 Lines.

The most basic structure used in electronic and physical characterization is the line [45]. In this thesis, the term ‘line’ is used to refer to a quasi-one dimensional physical structure, where the structure length is much greater than the width and the height. In the tests described in this paper, line heights are less than 50 nm, but vary with the number of layers printed. The typical line described in this paper has a width of 1 mm and a length ranging from 3 mm to 15 mm.

A line is simple and straightforward to construct when using the Dimatix [45]. Because it is the elementary building block of electronics, the line has many useful applications. Printed SWCNT lines can act as wires, interconnects, and antennas. Before curved sections and other more complex structures are characterized, the line needs to be characterized to provide a baseline for comparison. Due to this fact, the electrical and physical characterization of a printed SWCNT line will be useful to future research and applications.

3.3.2 Rectangles.

Rectangles are the two-dimensional structures in which the length and width take on sizes that are comparable. In this thesis, printed rectangles measured between 0.5 and 5 mm on each side.

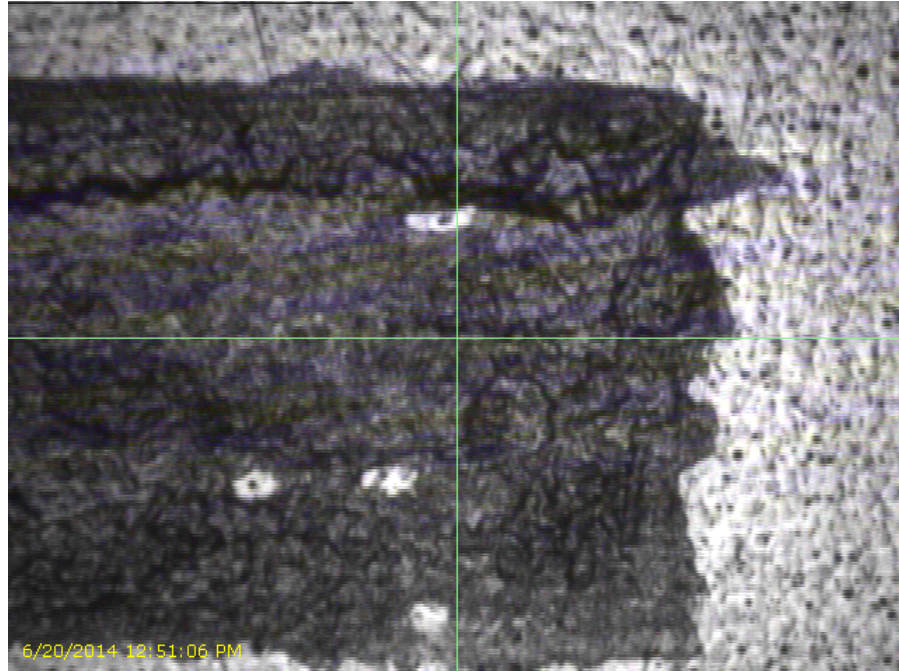


Figure 3.4: Printed line on polyimide.

As with lines, the height of the rectangle is related to the number of layers printed. The printed rectangle is used to test nearly simultaneous sheet resistances at right angles from each other. The sheet resistance of the printed rectangle is measured across the face of the rectangle and recorded. The sample is then rotated ninety degrees clockwise and the sheet resistance is measured again, recorded, and compared to the original data.

3.3.3 *Coplanar Waveguides*.

CPWs consist of three parallel transmission lines on the same plane. The outer lines are ground lines, while the center line is the signal line. Figure 3.6 shows a CPW. The ideal CPW consists of a signal line and two infinite planes which serve as ground lines. This is impossible to implement, so the ground lines are made to be significantly wider than the signal line to function as a nominally infinite plane. In this work, a 250 micron pitch was used, which corresponds to a signal line width of 100 μm , a gap width of 100 μm , and ground line width of 250 μm . Due to the fact that CNTs exhibit contact and

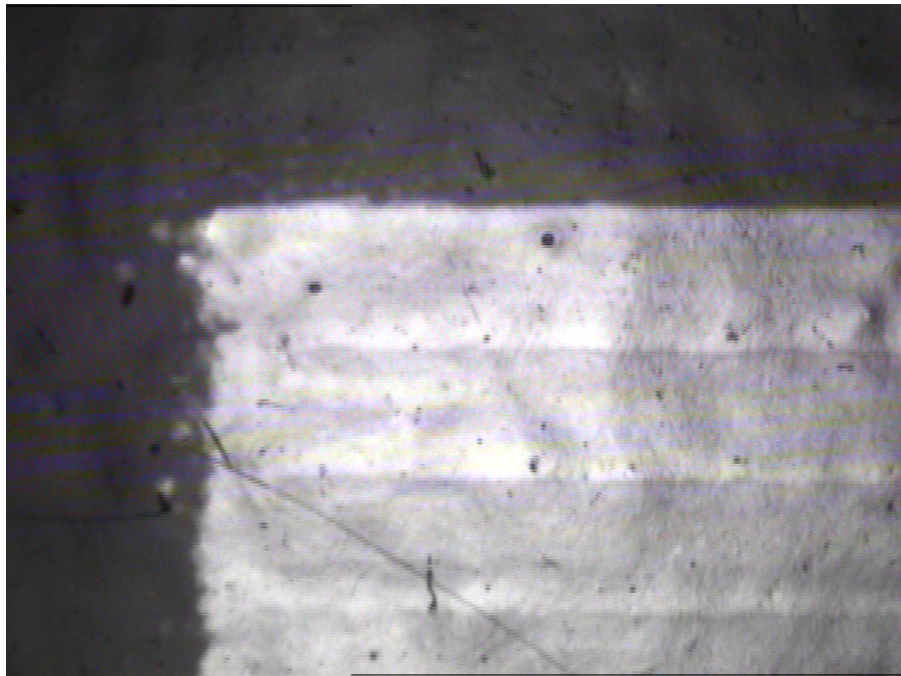


Figure 3.5: Printed square on paper.

transmission resistance, the CPWs printed in this research are expected to exhibit insertion and transmission losses of at least -10 dB. Figure 3.7 shows a printed CPW.

3.3.3.1 CPW with Silver.

A secondary CPW design was used in testing. This design consisted of the original CPW discussed in Section 3.3.3 with silver ink deposited as contact pads on the transmission line. The silver ink formed a physical buffer between the probes and the CNT transmission lines. The ground lines in the secondary CPW design were printed with silver ink instead of CNT ink. The added silver in the secondary design was to remove any uncertainty caused by possibly inefficient transmission of current by the CNT ground lines. The silver contact pads were designed to be more resistant than the CNTs to possible damage caused by the probes used by the network analyzer.

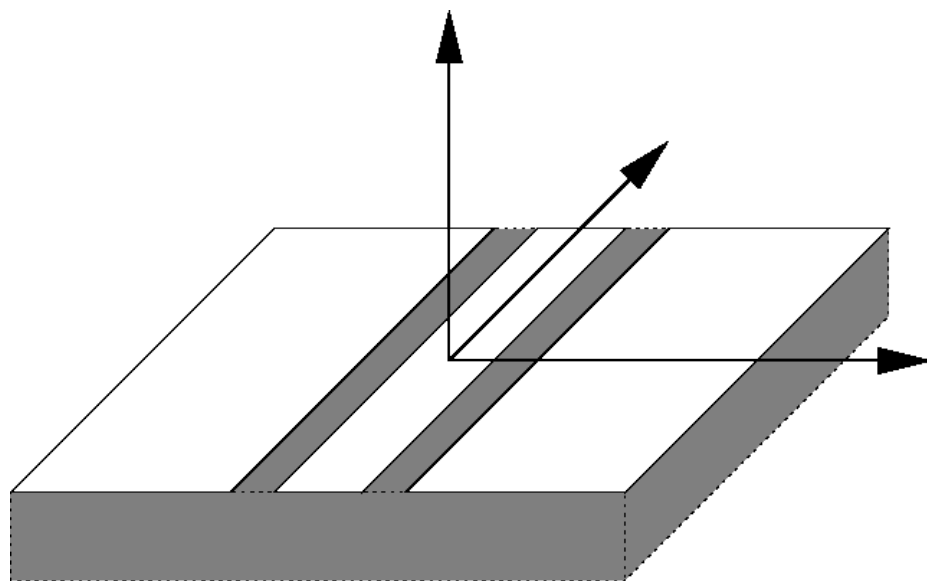


Figure 3.6: A standard CPW with a juxtaposed axis system [50].

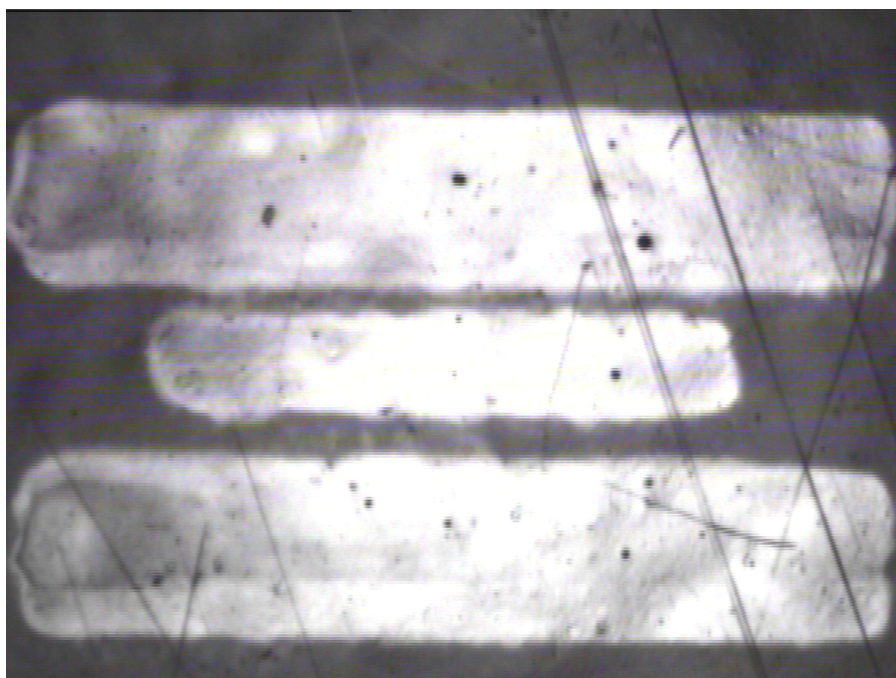


Figure 3.7: Printed CPW on paper.

3.3.4 Inductors.

For the purposes of this research, inductors consist of a continuous transmission line formed into a square spiral. Figure 3.8 shows an inductor. The following dimensions

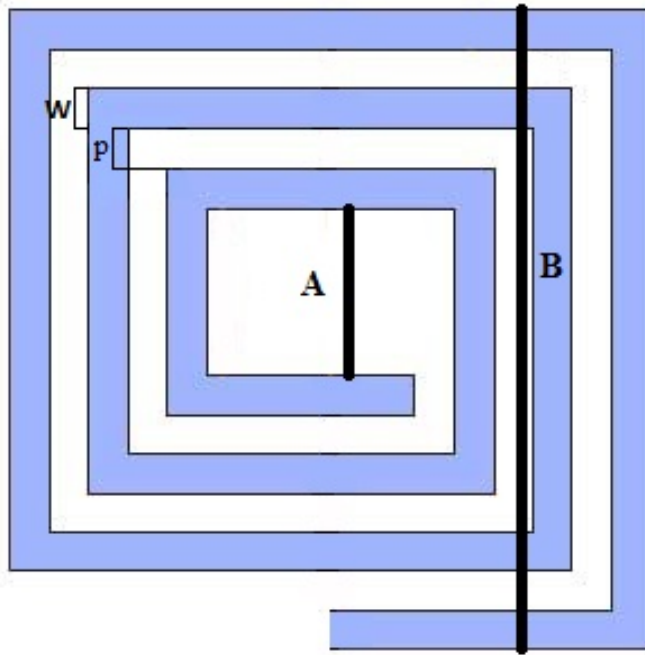


Figure 3.8: A square spiral inductor.

were used when printing inductors in this research: $w = p = 300 \mu\text{m}$; $A = 1200 \mu\text{m}$; $B = 4800 \mu\text{m}$. All inductors used in this research were printed on glass using the Optomec aerosol jet printer. The inductors in this research were expected to have values in the microhenry (μH) range.

3.4 Summary

Chapter 3 discussed the experimental methodology used in this research, to include the initial and primary test methodologies, the test subjects, and the tests needed to produce the required parameters for characterization. Section 3.2.1 dealt with the initial set-up and configuration of the Dimatix printer, as well as the initial testing of the Brewer

Science © Aerosol Jet ink and its subsequent failure in the Dimatix ink jet printer. Section 3.2.2 presented the tests and test equipment which was used to characterize the ink. The primary test methodology consists of testing printed lines, squares, and CPWs to determine values for the parameters given in Section 3.2.2. Section 3.3 presented the printed circuits which were tested to characterize the electrical and physical properties of the ink.

IV. Analysis and Results

4.1 Chapter Overview

This chapter presents and discusses the results and analysis of this research. Section 4.2 outlines the general analysis and findings of this research. Section 4.2.1 discusses the viability of the various substrates used in this research. Sections 4.2.2 through 4.2.6 discuss the results of experimentation. Section 4.2.7 discusses the viability of the Brewer Science © CNT-based ink in printed electronic applications. Section 4.2.8 presents detailed specifications for the implementation of the test subjects used in this research. Section 4.3 gives a summary of Chapter 4.

4.2 Results of Experimentation

Section 4.2 presents and explains the results of the experimentation conducted during this research. The viability of various substrates, electrical and physical characteristics of the ink, and potential applications of the ink will be discussed.

4.2.1 Viability of Substrates.

During the experimentation process, data was collected on the substrates used in testing to develop a profile of their usefulness. The viability of paper, glass, polyimide, and nomex was ascertained. The conclusions given in this section concern the substrate listed when used with the Brewer Science © CNT-based ink and the Dimatix ink jet printer.

4.2.1.1 Paper.

Epson and HP brand high gloss photographic grade paper was used in this research. Circuits on paper substrates passed the tape test, but did not adhere completely when S-parameter tests were conducted. When the network analyzer's ground-signal-ground probes contacted the CPW transmission and ground lines, the lines separated from the paper and stuck to the probes. The accuracy of printed circuits on paper surpassed those on

glass and polyimide. Feature sizes as small as $50\text{ }\mu\text{m}$ were attained using paper substrates. The corners of lines printed on paper were square, barring the curvature of a single drop of ink. Rounding was present only on the scale of an individual drop of ink. The surface morphology of the circuits printed on paper was smooth, with no aberrations, streaking, or pitting visible under microscope inspection at 100x magnification. While using a vacuum oven to cure the printed circuits, temperatures above $120\text{ }^{\circ}\text{C}$ caused the paper substrate to curl in a convex manner in relation to the circuit. Due to the observations listed above, paper is a viable substrate for printing electronic circuits as long as high temperatures and physical stress will not be placed on the circuit, or if durability under high stress or temperature is not a design constraint.

4.2.1.2 *Glass.*

Three types of glass were used in this research: untreated silicon dioxide glass, plasma ashed glass, and hexamethyldisilazane (HMDS) coated quartz. Circuits printed on all three glasses passed the tape test. Ink adherence was not shown to be diminished by heat, vacuum, or physical contact including metallic ground-signal-ground probes. Due to the low porosity of glass when compared to paper, longer drying times and higher platen and cartridge temperatures were used when printing ink on glass substrates. See Tables 4.3, 4.4, and 4.5 for a comparison of drying times and platen and cartridge temperatures used in printing on various substrates. The accuracy with which the ink could be printed on glass substrates varied with the type of glass. However, printed ink showed a tendency to flow on all types of glass, rounding out corners that were designed to be square. On untreated glass, the ink pooled and dried in a circular coffee-ring pattern. Due to the coffee ring pattern and the relative disparity of ink thickness between the center and edges of a pattern, design sizes increased by approximately 50% before drying. Feature sizes smaller than $300\text{ }\mu\text{m}$ for a single layer and $500\text{ }\mu\text{m}$ for three layers were not attainable on untreated glass. The coffee-ring effect was not noticeable on plasma ashed glass. Correspondingly,

no expansion of printed lines was noticed. A line designed to be 1 mm wide dried at 1 mm wide. While the increased accuracy allowed for lines to be accurately printed, the feature sizes of ink printed on plasma ashed glass were not small enough to allow for a CPW to be printed. The signal and ground lines merged together due to the ink's tendency to flow. HMDS quartz was only used in conjunction with a shadow mask in an attempt to print an interdigitated capacitor. The ink adhered to the substrate, but the mask interfered with the pattern, preventing useful data from being collected concerning feature size, surface morphology, and accuracy. Based on the data above, it is seen that glass is a viable substrate under particular conditions. When the glass is plasma ashed to increase the surface energy, glass becomes a viable substrate as long as feature sizes smaller than half a millimeter are not needed. However, the tendency of ink on glass to flow creates problems with design accuracy. Due to its rigidity and durability, glass presents advantages over paper as a substrate when strength is desired over flexibility. Glass can also withstand much higher temperatures than paper.

4.2.1.3 Polyimide.

Circuits on polyimide substrates passed the tape test. The accuracy of printed circuits on polyimide mirrored that of printed circuits on ashed glass. Feature sizes were comparable and the corners of lines printed on polyimide were rounded instead of square. As with glass substrates, the obtainable accuracy and feature sizes of ink printed on polyimide prevented the implementation of a CPW. Ink printed on polyimide showed less coffee-ringing than glass. However, the interior area of printed 1 mm by 5 mm lines showed significant pooling of ink, resulting in banded and dappled patterns. This resulted in a lack of conductance along the length of the line, as a conducting path of even composition was not apparent. The polyimide substrates showed no vulnerability to the 120 °C temperatures used in the vacuum baking process. Due to the observations listed above, polyimide is not a viable substrate for printing electronic circuits. While the accuracy and feature size

is comparable to that of ink printed on ashed glass, the banding apparent on polyimide negates the ink's ability to be used as a conductor.

4.2.1.4 *Nomex* © .

Sheets of Dupont brand Nomex © were used in this research. Circuits on Nomex © substrates passed the tape test. The accuracy of circuits printed on Nomex © was equal to that of those printed on paper. Feature sizes as small as $50 \mu\text{m}$ were attained using Nomex © substrates. The surface morphology of the circuits printed on Nomex © was smooth, with no aberrations, streaking, or pitting visible under microscope inspection at 100x magnification. The corners of lines printed on Nomex © were square, barring the curvature of a single drop of ink. Rounding was present only on the scale of an individual drop of ink. The Nomex © substrate was resistant to the 120°C used to vacuum bake the printed circuits. Due to the observations listed above, Nomex © is a viable substrate to be used in printed electronic applications. Its flexibility and strength make it more durable than paper. It is also more resistant to heat than paper substrates.

4.2.2 *Thickness of Deposited Ink.*

Each substrate used in this research can be described with a surface roughness. Surface roughness is the amount of vertical separation between the lowest and highest points on the substrate surface. This roughness is measured with a stylus profilometer. A range of roughnesses is determined based on multiple profilometer passes on multiple samples of each substrate. Table 4.1 gives the range of surface roughnesses for each substrate used in this research. The most accurate profilometer used in this research could not detect a nine layer printed line on ashed glass, due to the surface roughness of the glass substrate. Therefore, the actual thickness of nine printed layers on ashed glass is estimated to be significantly less than 50 nm. Following this estimation and the tendency of printed ink to flow before it completely dries, the maximum possible thickness of CNT ink deposited via ink jet printing is estimated to be on the order of 50 nm. The thickness of CNTs

deposited on paper, polyimide, and Nomex © could not be measured due to the relatively high surface roughness compared to glass. However, it is reasonable to estimate that the thickness of the CNTs deposited on paper, polyimide, or Nomex © does not exceed the thickness of the CNTs printed on glass. Future measurements of the thickness of the deposited ink should be completed using atomic force microscopy or interferometry.

Table 4.1: Surface Roughness of Paper, Glass, Polyimide, and Nomex ©

| Substrate | Surface Roughness |
|------------------|--------------------------|
| Paper | 500-750 nm |
| Polyimide | 400-600 nm |
| Glass | 50-100 nm |
| Nomex © | 1100-1500 nm |

4.2.3 Sheet Resistance.

Sheet resistance was shown to decrease as the thickness of the printed sample increased. The most significant decrease corresponded to the increase in thickness from 1 to 3 printed layers. Each successive printed layer decreased the sheet resistance by a smaller margin. The decrease in sheet resistance was still apparent at eleven printed layers, but its effect was marginal. The sheet resistance of printed lines on paper is shown in Figure 4.1. The units on the vertical axis are $k\Omega/\square$, while the horizontal axis gives the number of layers printed. The exact recorded data is displayed next to each data point. The results from the first test are displayed to the left of the trend line. The results from the second test are displayed above the trend line. Similar results were recorded from CNTs deposited on a Nomex © substrate using the ink jet printer. Figure 4.2 shows the sheet resistance of printed lines on Nomex ©. The units on the vertical axis are $k\Omega/\square$, while the horizontal axis gives the number of layers printed. The exact recorded data is

displayed next to each data point. The sheet resistance data taken from CNT lines printed on polyimide were unrepeatable due to the incongruent nature of the deposited CNTs. The measured sheet resistance fluctuated between the $M\Omega/\square$ range and values too high for the four point probe to accurately measure.

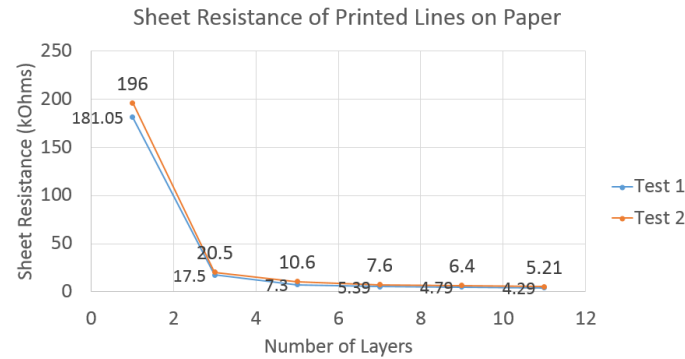


Figure 4.1: Sheet resistance of printed lines on paper.

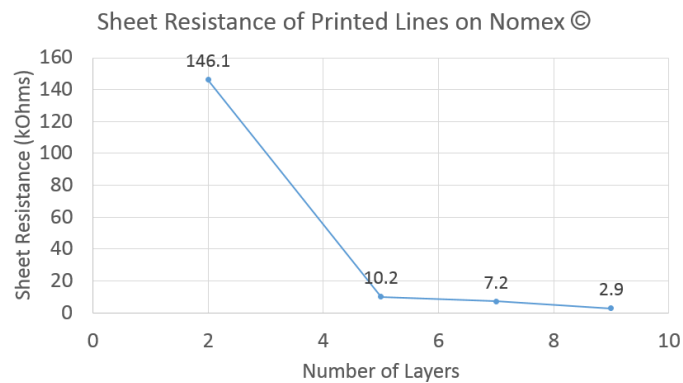


Figure 4.2: Sheet resistance of printed lines on Nomex ©.

4.2.3.1 Resistivity and Sheet Resistance.

Resistivity can be directly calculated from sheet resistance. The sheet resistance (R_{\square}) of a material is the material's resistivity (ρ) divided by the thickness. Equation 4.1

shows the calculation of sheet resistance from resistivity. A material's resistance (R) is its resistivity (ρ) multiplied by its length (L), divided by its cross-sectional area (A). Equation 4.2 shows the calculation of resistance from resistivity.

$$R_{\square} = \frac{\rho}{t} \quad (4.1)$$

$$R = \rho \frac{L}{A} \quad (4.2)$$

4.2.3.2 Resistivity of Aerosol Jet Printed Ink.

As a comparison to the ink jet deposition method, lines and CPWs were printed on glass using the aerosol jet printer and the Brewer Science © CNT ink formulation. These aerosol jet printed transmission lines showed much lower resistivities than those lines printed on the ink jet printer. Lines printed with the aerosol jet printer on glass with a thickness of approximately 800 nm had a sheet resistance on the order of 5-7 Ω/\square .

4.2.3.3 Conductivity.

Conductivity relates directly to resistivity in that conductivity is the inverse of resistivity. Conductivity, expressed in *siemens*, can be calculated as:

$$G = \frac{1}{\rho} \quad (4.3)$$

where G is conductivity, and ρ is resistivity.

4.2.4 S-parameters.

In this research, printed CPWs were assumed to be perfectly symmetric. The S-parameters of the printed CNT-based ink were taken in three stages. The first stage used test subjects printed with the Dimatix ink jet printer on paper. Figures 4.3 and 4.4 show the rectangular and Smith chart plots of $S[1,1]$ for a CPW of 9 layers. Because the nearly-open transmission line in Figure 4.4 exists in the top half of the Smith Chart, the test subject can be deduced to be inductive. The effects of the inductive nature of the test subject can be seen in the noise in Figure 4.3. The second stage for the collection of S-parameters used test subjects printed with an aerosol jet printer on glass. These CPWs were roughly 300 nm

thick. The third stage for the collection of S-parameters used test subjects printed with an aerosol jet printer on glass. These CPWs were roughly 780 nm thick. The only difference in the 300 nm and 780 nm thick samples is the number of layers used to deposit the ink. The results from the S-parameter tests for stages two and three can be seen in Figures 4.5 and 4.6. Figures 4.5 and 4.6 show much better S-parameter results for the aerosol jet printed samples than the ink jet printed samples. Insertion and transmission losses are between 5 dB and 10 dB for CPWs with a thickness of 780 nm. The reflection of the thicker CPW is also lower than the thinner CPWs. For the 780 nm thick sample, measurements were taken at three points on the CPW. An outside measurement was taken at the full length of the CPW, an inner measurement was taken with the probes as close as possible without touching, and a middle measurement was taken with the probes equidistant between the inner and outer positions. The CPWs in this research were not designed to have matched loads, as the ink used to print them had not yet been characterized. This introduced some amount of error as the mismatched loads and changing distances between the probes could alter the transmission and reflection results.

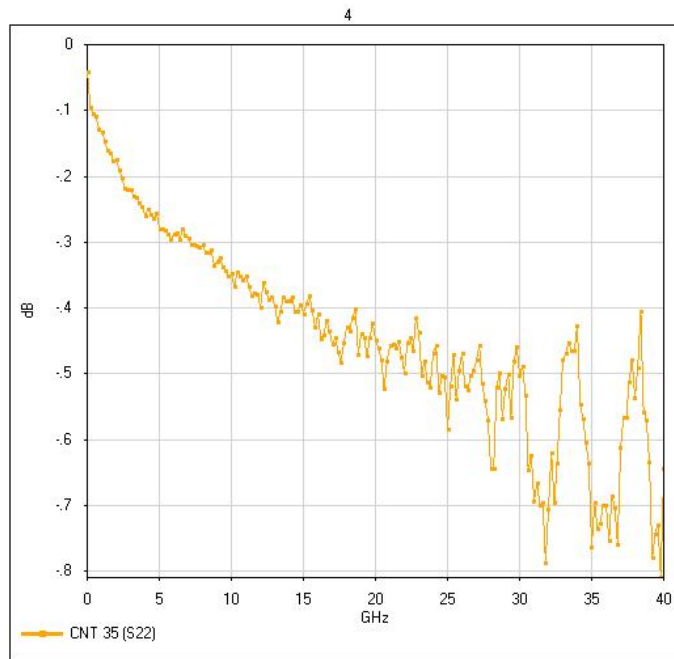


Figure 4.3: Rectangular chart plot of $S[1,1]$ for sample 35, a CPW of 9 layers.

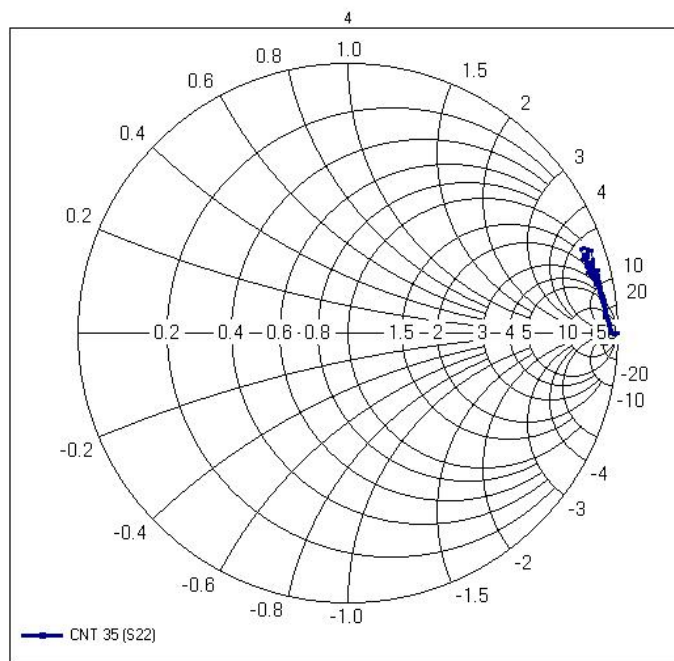


Figure 4.4: Smith chart plot of $S[1,1]$ for sample 35, a CPW of 9 layers.

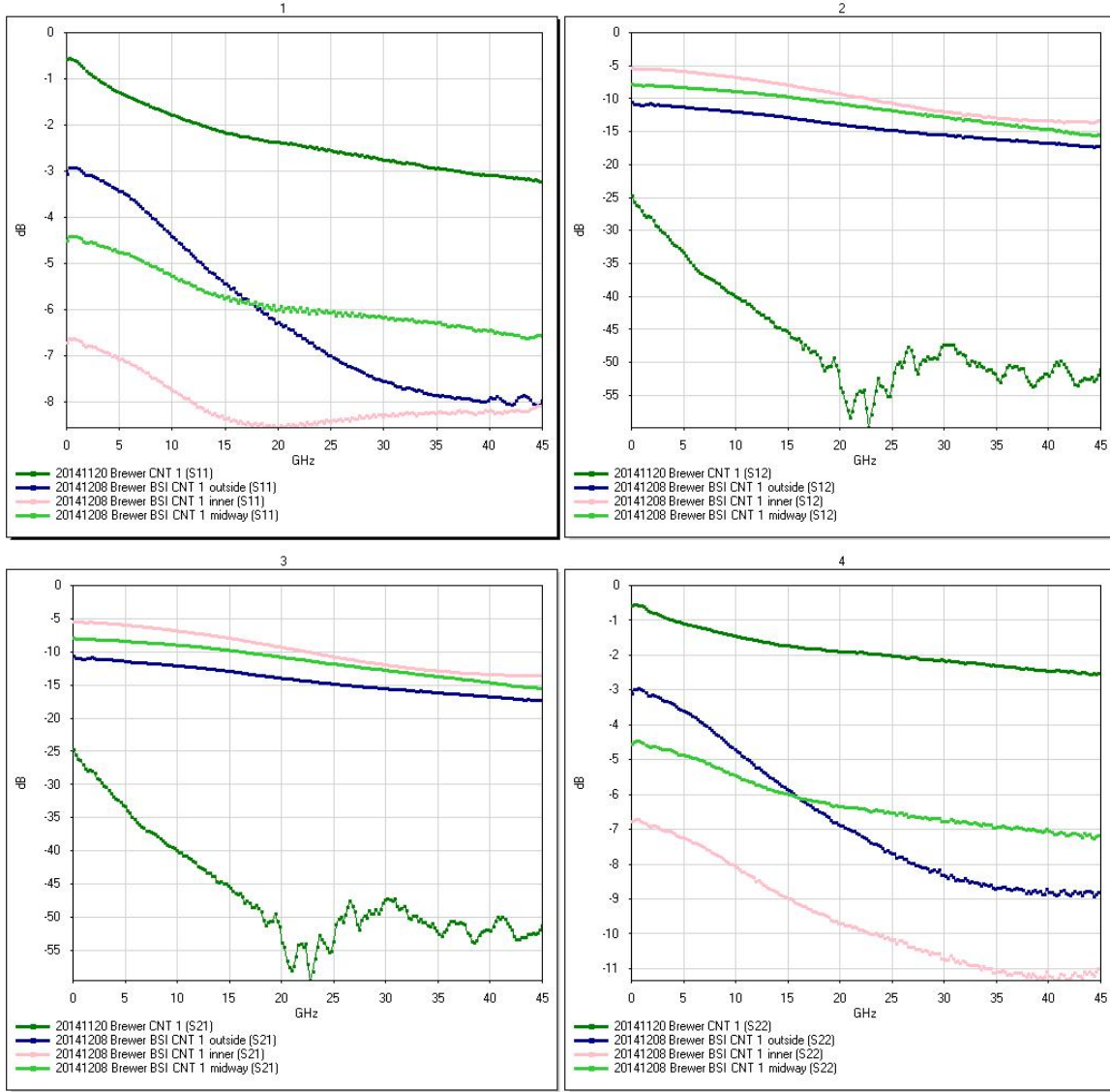


Figure 4.5: Rectangular chart plots of S-parameters for CPWs printed with an aerosol jet printer. CNT 1 represents a CPW with a thickness of 300 nm. CNT 1 outside, CNT 1 inner, and CNT 1 midway are plots from a single CPW with a thickness of 780 nm. CNT 1 outside represents measurements taken across the full length of the CPW. CNT 1 midway represents measurements taken across half of the CPW. CNT 1 inner represents measurements taken across a minimal distance of the CPW.

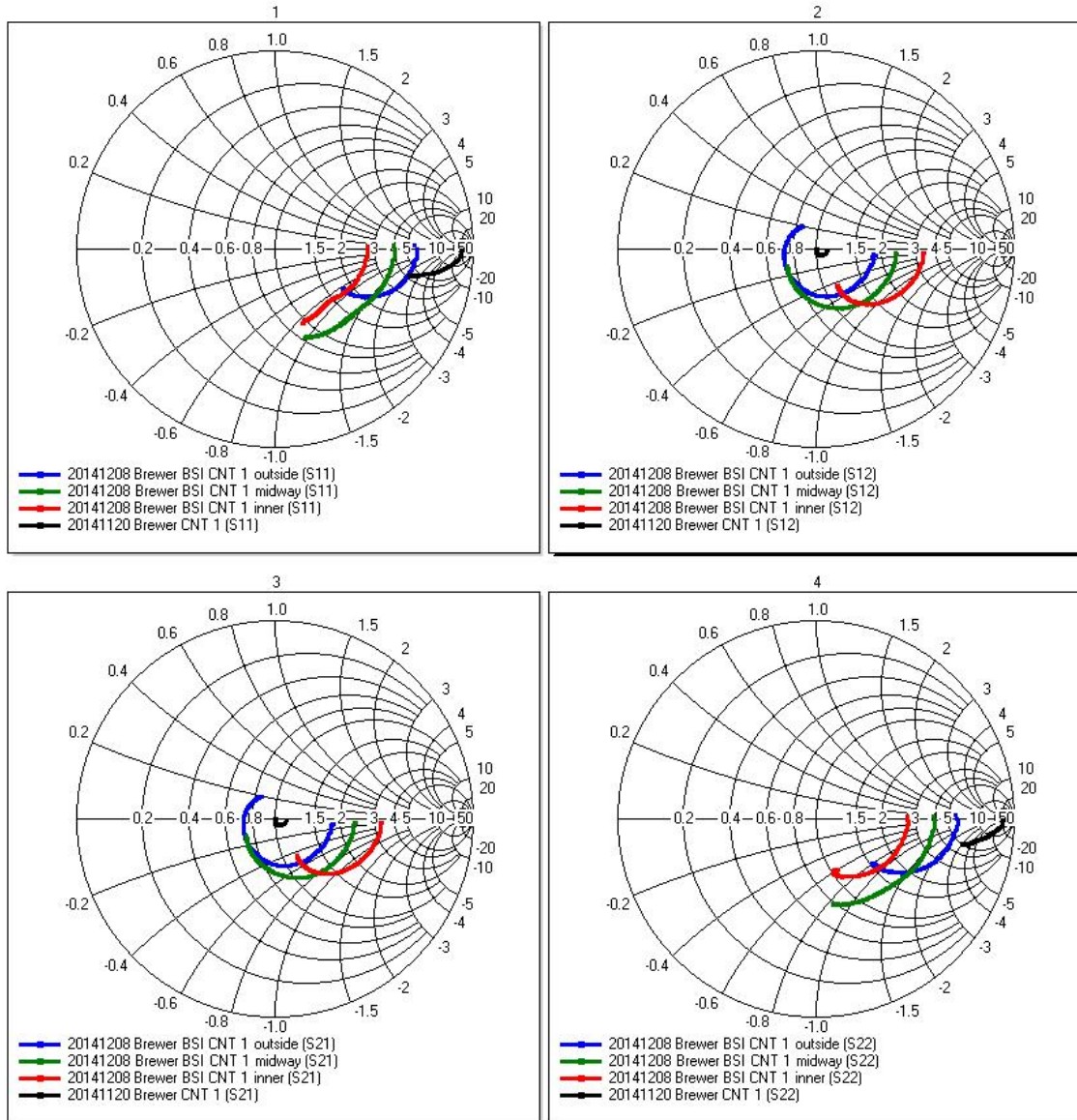


Figure 4.6: Smith chart plots of S-parameters for CPWs printed with an aerosol jet printer. CNT 1 represents a CPW with a thickness of 300 nm. CNT 1 outside, CNT 1 inner, and CNT 1 midway are plots from a single CPW with a thickness of 780 nm. CNT 1 outside represents measurements taken across the full length of the CPW. CNT 1 midway represents measurements taken across half of the CPW. CNT 1 inner represents measurements taken across a minimal distance of the CPW.

4.2.4.1 Effect of Thermal Bias on S-parameters.

The effect of temperature on the S-parameters of a printed CPW was determined by subjecting the sample to a thermal bias. The metallic chuck on which the sample rested was heated to 25 °C, 50 °C, 75 °C, 100 °C, and 150 °C. Once each temperature was reached, S-parameter measurements were taken at that temperature. No change was noted between the given temperatures. The results from the S-parameter tests can be seen in Figures 4.5 and 4.6. The Brewer Science © CNT-based ink was not temperature dependent up to 150 °C.

4.2.4.2 Effect of Electric Field Bias on S-parameters.

The effect of an electric field on the S-parameters of a printed CPW was determined by subjecting the sample to an electric field bias. Electric potentials of 0V, 5V, 10V, 15V, and 20V, were applied across the metallic chuck on which the sample rested. The sample was printed on a 50 μ m thick sheet of polyimide which rested directly on the chuck. The bias of the electric field was determined to have no effect on the S-parameters of the CPW, possibly due to the fact that the distance between the field's source and the test subject was too great. It was not possible to apply an electric potential directly to the transmission line of the CPW, because the network analyzer used did not have a way to absorb the DC offset generated by such a voltage. One method to decrease the distance between the CPW and the material used to generate the electric field would be to use a conductive substrate with a thin, non-conductive oxide layer coat. Printing on this oxide layer would put the CPW much closer to the electric field.

4.2.5 Fourier Transform Infrared Spectroscopy.

FTIR data was collected to determine the transparency of the CNT-based ink. The ink was deposited using the Optomec © aerosol jet printer. Two samples were produced, one with four passes of the print head (4 printed layers) and one with eight passes of the print head (8 printed layers). The sample deposited with four passes was 113.4 nm thick and

had a sheet resistance of $17.3 \Omega/\square$. The sample deposited with eight passes was 213.4 nm thick and had a sheet resistance of $11.8 \Omega/\square$. Figure 4.7 shows the transmission data for the Brewer Science © CNT-based ink. As expected, the thicker sample was less transparent. The thinner sample had a maximum optical transmission value of 70.3%. Maximum transmission occurred at the wavelength of $2.19\mu m$. This wavelength corresponds to the low end of the middle band of the infrared spectrum. The peak transmission value sharply decreased at higher and lower wavelengths. Figures 4.8 and 4.9 show SEM images of CNTs printed on silicon nitride coated silicon using the aerosol jet printer.

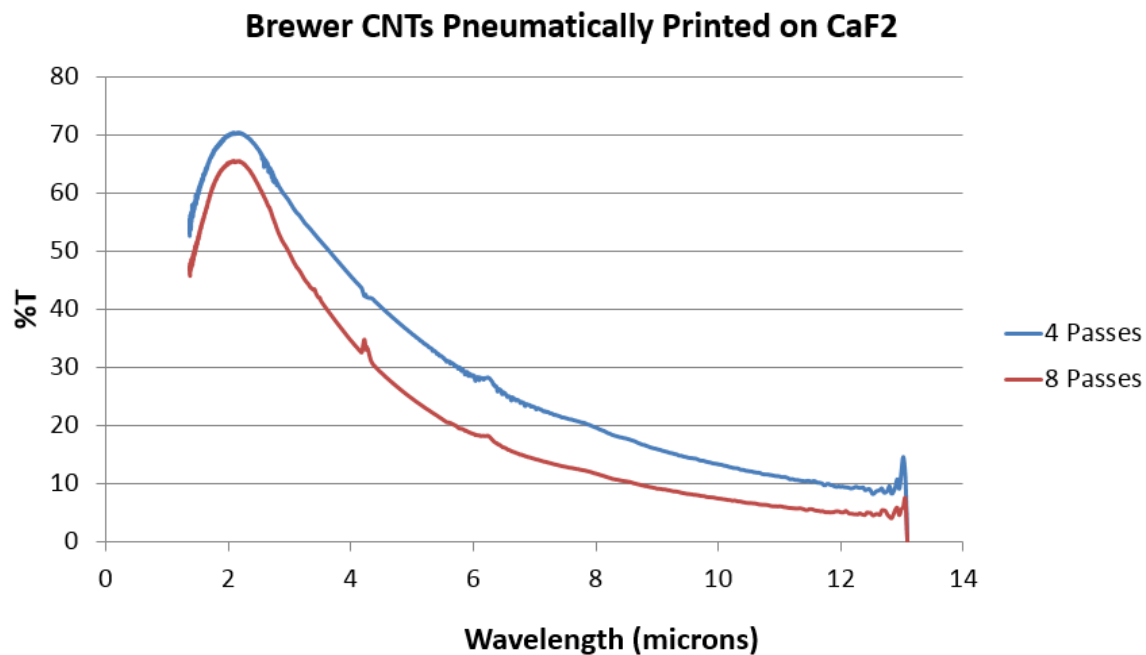


Figure 4.7: FTIR data for the Brewer Science © CNT-based ink.

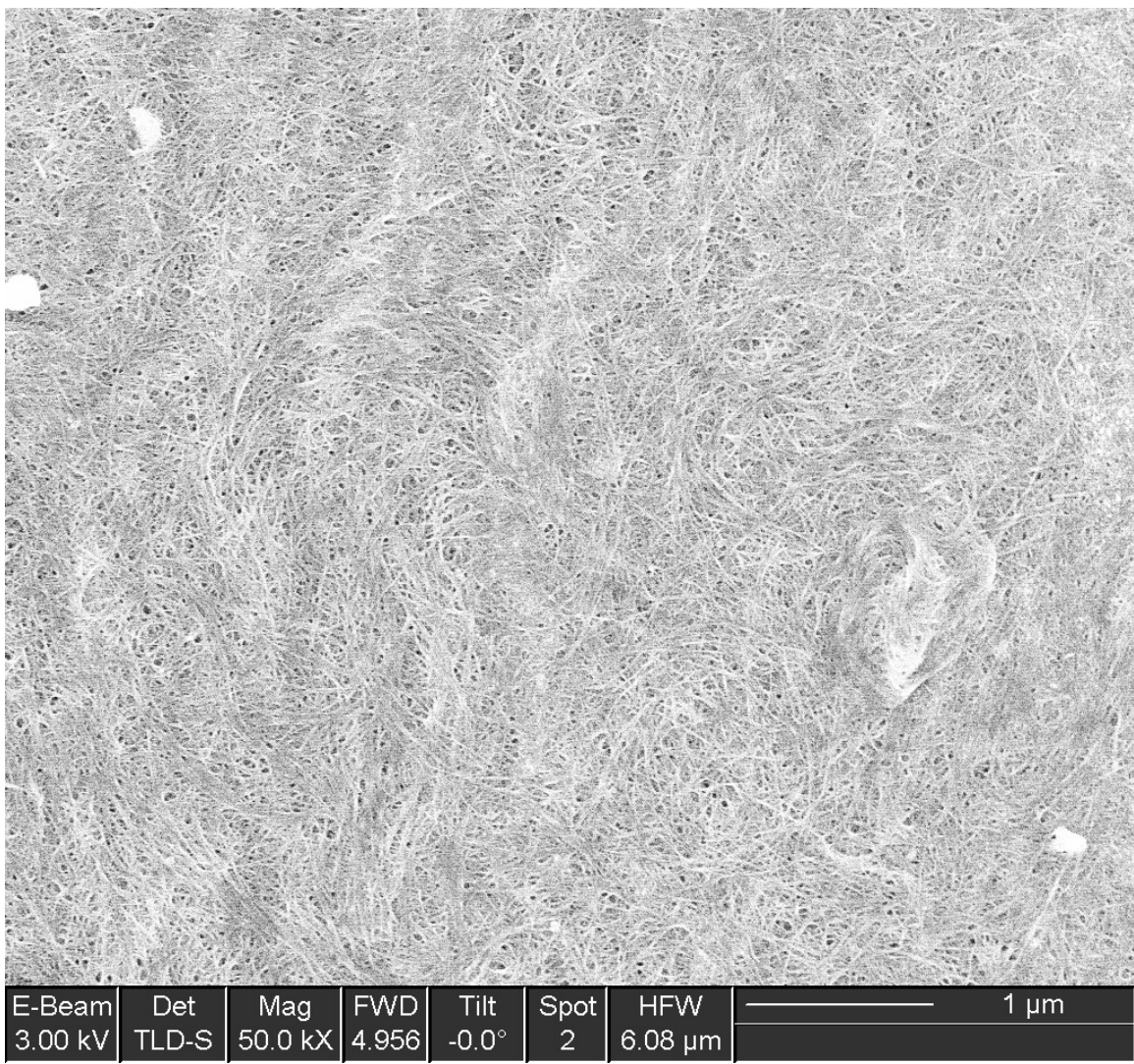


Figure 4.8: SEM image under 50kX magnification of CNT ink printed on silicon nitride coated silicon using the aerosol jet printer.

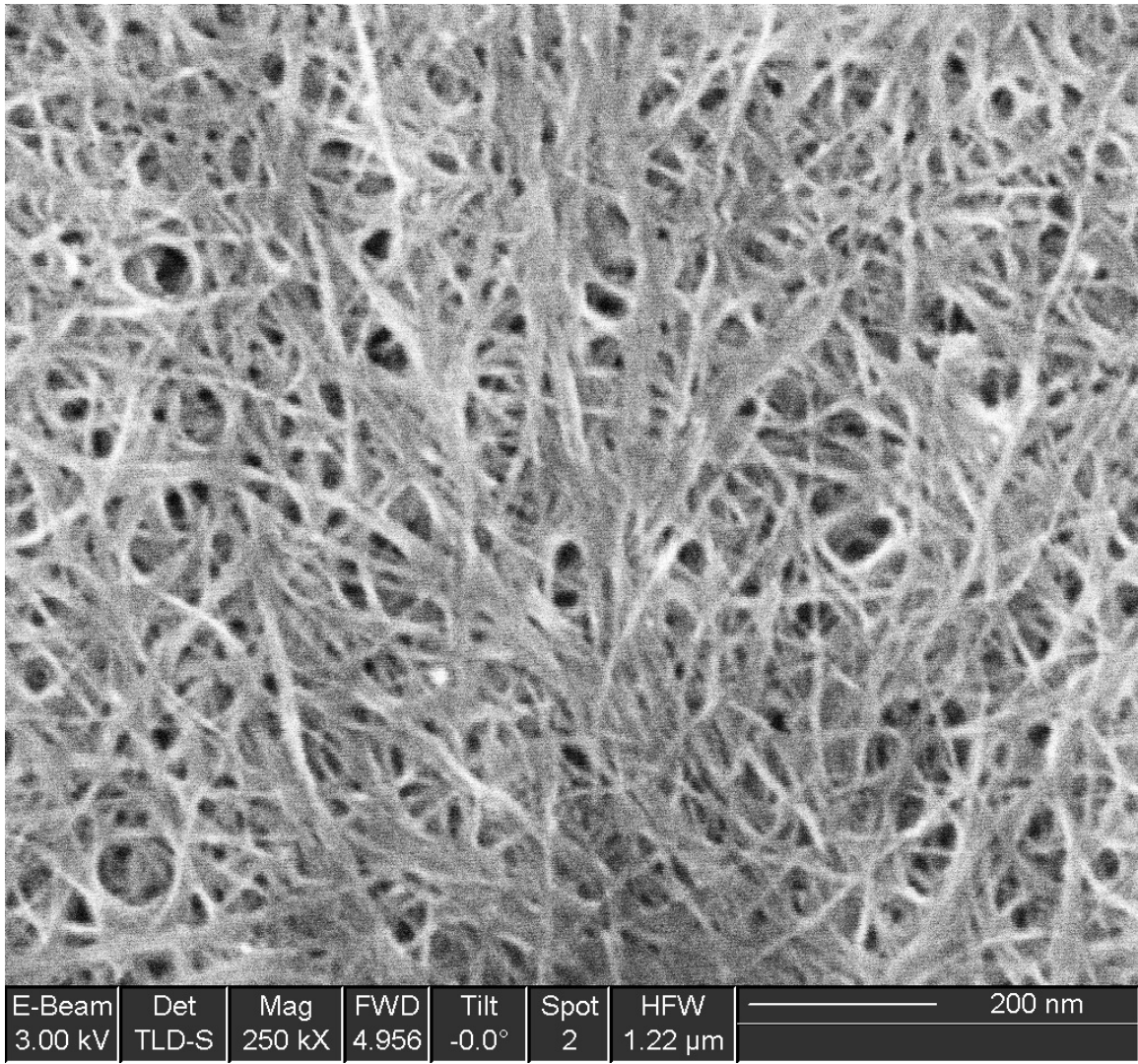


Figure 4.9: SEM image under 250kX magnification of CNT ink printed on silicon nitride coated silicon using the aerosol jet printer.

4.2.6 Inductance.

Inductors were printed on glass using the aerosol jet printer. Table 4.2 gives the thickness, series resistance, and series inductance of each printed inductor. Inductance was found to increase as thickness decreased. Increasing inductance and decreasing thickness were also found to correlate to increasing resistance. In Table 4.2, the column labeled “High,” is the maximum thickness of the sample. The column labeled “Low,” is the

minimum thickness of the sample. The column labeled “Average,” is the mean thickness of the sample. Note that sample number five has a minimum thickness of 0 nm. This is because the ink deposited on this sample contained a higher concentration of water than the other samples. The high concentration of water caused the ink to form beads before drying, resulting in a partial coating of the substrate. The maximum and average thicknesses of sample five are greater than the maximum and average thicknesses of samples three and four. The inductance of sample five is approximately 100 times greater than the inductances of samples three and four. This is the result of the ink beading and drying in a non-uniform pattern. The results given in Table 4.2 were collected using a 1 MHz, 1 volt carrier wave with no DC bias. The Q factor of the inductors designed and tested in this research was found to be between 0.01 and 0.03. A signal generator and an Inductance-Capacitance-Resistance (LCR) meter were used to test the performance of the inductors in this research.

Table 4.2: Thickness and Series Inductance and Resistance of Printed Inductors on Glass.

| Thickness | | | | | |
|---------------|--------------|----------------|----------|---------|---------|
| Sample Number | Ls | Rs | High | Low | Average |
| 1 | $1.4\mu H$ | $1.28k\Omega$ | $2261nm$ | $300nm$ | $400nm$ |
| 2 | $890nH$ | $2.24k\Omega$ | $1600nm$ | $100nm$ | $200nm$ |
| 3 | $16.4\mu H$ | $7.36k\Omega$ | $573nm$ | $65nm$ | $115nm$ |
| 4 | $59.7\mu H$ | $17.0k\Omega$ | $525nm$ | $70nm$ | $120nm$ |
| 5 | $905.5\mu H$ | $77.64k\Omega$ | $860nm$ | $0nm$ | $235nm$ |

4.2.7 *Viability of the Brewer Science © CNT-based Ink.*

Two inks were used in this research. One was designed for the ink jet printer and one was designed for the aerosol jet printer. Both inks were a custom formulation of CNTs.

They were not the COTS screen printing ink which Brewer Science © sells. Overall, the Brewer Science © CNT-based ink jet ink exhibited characteristics which make it difficult to use in most applications. Of primary importance is the relatively resistive nature of the ink. Metal conductors have sheet resistances on the order of $5 \Omega/\square$. The ink tested in this research exhibited a sheet resistance at least three orders of magnitude higher, when tested at thicknesses less than 50 nm. While the Brewer Science © ink is much more resistive than most conductors, it is not resistive enough to be used as a resistor in semiconductor applications. Another point to consider is the S-parameters of the deposited ink. As discussed in Section 4.2.4, the waveguides printed using the CNT-based ink and the ink jet printer show high insertion and transmission losses. These losses detract from their viability. Despite the areas in which the Brewer Science © CNT-based ink exhibited characteristics as expected, the resistive and lossy nature of the ink severely limits its practical applications, especially when printed with the Dimatix ink jet printer. At the conclusion of this research, Brewer Science © informed us that the ink shipped to us for use in the aerosol jet printer coagulated in transport. This fact was unknown when the ink was printed, so for the purpose of this research, the ink was diluted with water. This altered the ink's performance.

4.2.8 Test Subjects by Reference Number.

Tables 4.3, 4.4, and 4.5 give the pertinent parameters for each sample printed and tested on the ink jet printer.

Table 4.3: Detailed Parameters for All Printed Test Subjects.

| R # | Shape | Substrate | Space | P Temp | C Temp | Layers | Delay |
|-----|-------------------|-------------|------------------|--------|--------|--------|--------|
| 1 | 1 x 5 mm rect | Photo paper | 30 μm | 40 °C | 35 °C | 1 | |
| 2 | 1 x 5 mm rect | Photo paper | 30 μm | 40 °C | 35 °C | 3 | 10 sec |
| 3 | 1 x 5 mm rect | Photo paper | 30 μm | 35 °C | 35 °C | 1 | |
| 4 | 1 x 5 mm rect | Photo paper | 30 μm | 35 °C | 35 °C | 3 | 10 sec |
| 5 | 1 x 5 mm rect | Photo paper | 30 μm | 35 °C | 35 °C | 5 | 10 sec |
| 6 | 1 x 5 mm rect | Photo paper | 30 μm | 35 °C | 35 °C | 7 | 10 sec |
| 7 | 1 x 5 mm rect | Photo paper | 30 μm | 35 °C | 35 °C | 9 | 10 sec |
| 8 | 1 x 5 mm rect | Photo paper | 30 μm | 35 °C | 35 °C | 11 | 10 sec |
| 9 | 0.5 x 0.5 mm rect | Polyimide | 40 μm | 40 °C | 35 °C | 1 | |
| 10 | 0.5 x 0.5 mm rect | Polyimide | 30 μm | 40 °C | 35 °C | 1 | |
| 11 | 0.5 x 0.5 mm rect | Polyimide | 22 μm | 50 °C | 35 °C | 1 | |
| 12 | 1 x 5 mm rect | Polyimide | 22 μm | 50 °C | 35 °C | 3 | 35 sec |
| 13 | 1 x 5 mm rect | Polyimide | 22 μm | 50 °C | 35 °C | 5 | 35 sec |
| 14 | 1 x 5 mm rect | Polyimide | 22 μm | 50 °C | 35 °C | 7 | 35 sec |
| 15 | 1 x 5 mm rect | Polyimide | 22 μm | 50 °C | 35 °C | 9 | 35 sec |
| 16 | 0.5 x 3 mm rect | Photo paper | 30 μm | 40 °C | 40 °C | 1 | |
| 17 | 0.5 x 3 mm rect | Photo paper | 30 μm | 40 °C | 40 °C | 3 | 10 sec |
| 18 | 0.5 x 0.5 mm rect | Glass | 60 μm | 25 °C | 35 °C | 3 | 10 sec |
| 19 | 1 x 5 mm rect | Glass | 60 μm | 25 °C | 35 °C | 5 | 10 sec |
| 20 | 1 x 5 mm rect | Glass | 60 μm | 25 °C | 35 °C | 7 | 10 sec |
| 21 | 1 x 5 mm rect | Glass | 60 μm | 25 °C | 35 °C | 3 | 10 sec |
| 22 | 1 x 5 mm rect | Glass | 60 μm | 25 °C | 35 °C | 9 | 10 sec |
| 23 | 1 x 5 mm rect | Photo paper | 30 μm | 30 °C | 35 °C | 1 | |
| 24 | 1 x 5 mm rect | Photo paper | 30 μm | 30 °C | 35 °C | 3 | 10 sec |
| 25 | 1 x 5 mm rect | Photo paper | 30 μm | 30 °C | 35 °C | 5 | 10 sec |
| 26 | 1 x 5 mm rect | Photo paper | 30 μm | 30 °C | 35 °C | 7 | 10 sec |
| 27 | 1 x 5 mm rect | Photo paper | 30 μm | 30 °C | 35 °C | 9 | 10 sec |

Table 4.4: Detailed Parameters for All Printed Test Subjects, Part 2.

| R # | Shape | Substrate | Space | P Temp | C Temp | Layers | Delay |
|------------|----------------------|------------------|------------------|---------------|---------------|---------------|--------------|
| 28 | 1 x 5 mm rect | Photo paper | 30 μm | 30 °C | 35 °C | 11 | 10 sec |
| 29 | 1 x 5 mm rect | Polyimide | 22 μm | 50 °C | 35 °C | 3 | 35 sec |
| 30 | 1 x 5 mm rect | Polyimide | 22 μm | 50 °C | 35 °C | 5 | 35 sec |
| 31 | 1 x 5 mm rect | Polyimide | 22 μm | 50 °C | 35 °C | 7 | 35 sec |
| 32 | 1 x 5 mm rect | Polyimide | 22 μm | 50 °C | 35 °C | 9 | 35 sec |
| 33 | CPW | Photo paper | 20 μm | 40 °C | 30 °C | 5 | 10 sec |
| 34 | CPW | Photo paper | 20 μm | 40 °C | 30 °C | 7 | 10 sec |
| 35 | CPW | Photo paper | 20 μm | 40 °C | 30 °C | 9 | 10 sec |
| 36 | CPW | Photo paper | 15 μm | 23 °C | 23 °C | 1 | |
| 37 | CPW | Photo paper | 15 μm | 23 °C | 23 °C | 1 | |
| 38 | CPW | Photo paper | 15 μm | 23 °C | 23 °C | 15 | 60 sec |
| 39 | CPW | Photo paper | 15 μm | 23 °C | 23 °C | 20 | 60 sec |
| 40 | CPW | Photo paper | 15 μm | 23 °C | 23 °C | 15 | 60 sec |
| 41 | 0.5 x 0.5 mm squares | Photo paper | 15 μm | 23 °C | 23 °C | 2 | 60 sec |
| 42 | 0.5 x 0.5 mm squares | Photo paper | 15 μm | 23 °C | 23 °C | 5 | 60 sec |
| 43 | 3 x 3 mm squares | Photo paper | 15 μm | 23 °C | 23 °C | 3 | 60 sec |
| 44 | 4 x 4 mm squares | Photo paper | 40 μm | 23 °C | 40 °C | 2 | 60 sec |
| 45 | 4 x 4 mm squares | Photo paper | 30 μm | 23 °C | 40 °C | 2 | 60 sec |
| 46 | 4 x 4 mm squares | Photo paper | 30 μm | 23 °C | 40 °C | 3 | 60 sec |
| 47 | 4 x 4 mm squares | Photo paper | 30 μm | 23 °C | 40 °C | 4 | 60 sec |
| 48 | 4 x 4 mm squares | Photo paper | 30 μm | 23 °C | 40 °C | 5 | 60 sec |
| 49 | 1 x 5 mm rect | Ashed Glass | 15 μm | 35 °C | 35 °C | 9 | 30 sec |
| 50 | 1 x 5 mm rect | Ashed Glass | 30 μm | 40 °C | 35 °C | 3 | 90 sec |
| 51 | 1 x 5 mm rect | Ashed Glass | 30 μm | 40 °C | 35 °C | 5 | 120 sec |
| 52 | 1 x 5 mm rect | Ashed Glass | 30 μm | 40 °C | 35 °C | 7 | 120 sec |

Table 4.5: Detailed Parameters for All Printed Test Subjects, Part 3.

| R # | Shape | Substrate | Space | P Temp | C Temp | Layers | Delay |
|------------|------------------|------------------|------------------|-----------------------|-----------------------|---------------|--------------|
| 53 | 1 x 5 mm rect | Ashed Glass | 30 μm | 60 $^{\circ}\text{C}$ | 35 $^{\circ}\text{C}$ | 3 | 150 sec |
| 54 | 1 x 5 mm rect | Ashed Glass | 30 μm | 60 $^{\circ}\text{C}$ | 35 $^{\circ}\text{C}$ | 5 | 180 sec |
| 55 | 1 x 5 mm rect | Ashed Glass | 30 μm | 60 $^{\circ}\text{C}$ | 35 $^{\circ}\text{C}$ | 7 | 180 sec |
| 56 | 1 x 5 mm rect | Ashed Glass | 30 μm | 60 $^{\circ}\text{C}$ | 35 $^{\circ}\text{C}$ | 9 | 180 sec |
| 57 | CPW | Photo paper | 20 μm | 23 $^{\circ}\text{C}$ | 40 $^{\circ}\text{C}$ | 1 | |
| 58 | CPW | Photo paper | 25 μm | 23 $^{\circ}\text{C}$ | 40 $^{\circ}\text{C}$ | 1 | |
| 59 | CPW | Photo paper | 30 μm | 23 $^{\circ}\text{C}$ | 40 $^{\circ}\text{C}$ | 1 | |
| 60 | CPW | Photo paper | 30 μm | 23 $^{\circ}\text{C}$ | 40 $^{\circ}\text{C}$ | 1 | |
| 61 | CPW | Photo paper | 30 μm | 35 $^{\circ}\text{C}$ | 40 $^{\circ}\text{C}$ | 5 | 60 sec |
| 62 | CPW signal line | Photo paper | 30 μm | 35 $^{\circ}\text{C}$ | 40 $^{\circ}\text{C}$ | 5 | 60 sec |
| 63 | CPW signal line | Photo paper | 30 μm | 35 $^{\circ}\text{C}$ | 40 $^{\circ}\text{C}$ | 5 | 60 sec |
| 64 | CPW signal line | Photo paper | 30 μm | 35 $^{\circ}\text{C}$ | 40 $^{\circ}\text{C}$ | 5 | 60 sec |
| 64 | CPW signal line | Photo paper | 30 μm | 35 $^{\circ}\text{C}$ | 40 $^{\circ}\text{C}$ | 5 | 60 sec |
| 65 | CPW signal line | Photo paper | 30 μm | 35 $^{\circ}\text{C}$ | 40 $^{\circ}\text{C}$ | 5 | 60 sec |
| 66 | 4 x 4 mm squares | Glass | 30 μm | 40 $^{\circ}\text{C}$ | 35 $^{\circ}\text{C}$ | 3 | 60 sec |
| 67 | 4 x 4 mm squares | HMDS Quartz | 30 μm | 40 $^{\circ}\text{C}$ | 35 $^{\circ}\text{C}$ | 3 | 60 sec |
| 68 | 4 x 4 mm squares | HMDS Quartz | 30 μm | 40 $^{\circ}\text{C}$ | 35 $^{\circ}\text{C}$ | 6 | 60 sec |
| 69 | 1 x 5 mm rect | Nomex | 30 μm | 40 $^{\circ}\text{C}$ | 35 $^{\circ}\text{C}$ | 2 | 180 sec |
| 70 | 1 x 5 mm rect | Nomex | 30 μm | 40 $^{\circ}\text{C}$ | 35 $^{\circ}\text{C}$ | 5 | 180 sec |
| 71 | 1 x 5 mm rect | Nomex | 30 μm | 40 $^{\circ}\text{C}$ | 35 $^{\circ}\text{C}$ | 7 | 15 sec |
| 72 | 1 x 5 mm rect | Nomex | 30 μm | 40 $^{\circ}\text{C}$ | 35 $^{\circ}\text{C}$ | 9 | 15 sec |

4.3 Summary

This chapter presented and discussed the results and analysis of this research. Section 4.2 discussed the general analysis and findings of this research to include electrical and physical characteristics of the deposited ink. Section 4.2.1 discussed the viability of the various substrates used in this research. Sections 4.2.2 through 4.2.6 discussed the results

of experimentation. Section 4.2.7 discussed the viability of the Brewer Science © CNT-based ink in printed electronic applications. Section 4.2.8 presented detailed specifications for the implementation of the test subjects used in this research.

V. Conclusions and Recommendations

5.1 Chapter Overview

This chapter presents the conclusion and recommendations of this research. Section 5.2 covers the investigative questions presented in Chapter 1 and presents answers to these questions based on research findings. Section 5.3 gives the conclusions of the research presented in previous chapters. Section 5.4 describes the significance of this research. Section 5.5 describes the future research that will benefit from or come about due to this research. Section 5.6 gives a summary of Chapter 5.

5.2 Investigative Questions Answered

As outlined in Chapter 1, the investigative questions posed by this research are as follows: What is the resistivity of the ink? What is the conductivity of the ink? What are the S-parameters of the ink? How do the electrical characteristics of the ink depend on the deposited ink's thickness? What is the minimum and maximum thickness with which the ink can be deposited? How uniformly can the ink be deposited? What is the surface morphology of the printed ink? How accurately can the ink be printed? How well does the ink adhere to its substrate? How does the substrate affect the questions asked above? In which applications can this ink be effectively used?

5.2.1 *Previously Answered Investigative Questions.*

The answers to some of the investigative questions have been given in previous sections. For answers concerning the resistivity of the ink, refer to Section 4.2.3. For answers concerning the conductivity of the ink, refer to Section 4.2.3.3. For answers concerning the S-parameters of the ink, refer to Section 4.2.4. For answers concerning the thickness of the printed ink, refer to Section 4.2.2. For answers concerning uniformity, surface morphology, accuracy, adherence, and substrate effects, refer to the appropriate

substrate discussion in Section 4.2.1. For answers concerning the applications of this ink, refer to Section 4.2.7.

5.2.2 Unanswered Investigative Question.

That leaves the question “How do the electrical characteristics of the ink depend on the deposited ink’s thickness?” to be discussed. As seen previously in the discussions of resistivity and S-parameters, the deposited ink’s thickness affects the electrical characteristics displayed. In the case of sheet resistance, as the thickness of the deposited material increases, the sheet resistance decreases. The inverse is true for conductivity. In the case of S-parameters, as the thickness increases, transmission ($S[2,1]$) increases and reflection ($S[1,1]$) decreases.

5.3 Conclusions of Research

The Brewer Science CNT-based inks were tested on a variety of substrates. The viability of paper, glass, nomex, and polyimide were determined under certain conditions. Paper and Nomex © were determined to be useful in applications where small feature size was not necessary. The applications of the Brewer Science inks when printed with the Dimatix ink jet printer were found to be trivial. When printed on paper, feature sizes as small as $50 \mu\text{m}$ were attained. These feature sizes are not small enough to accurately print devices such as CPWs and inductors. However, the ink jet printer could not deposit CNTs thick enough to permit the construction of a useful device. The applications of the Brewer Science ink when printed with the Optomec aerosol jet printer were demonstrated to include printed CPWs and inductors. The aerosol jet printer surpassed the ink jet in deposited ink thickness and electrical efficiency. The electrical and physical characteristics of the Brewer Science CNT-based ink were determined and reported. The ink was shown to have a sheet resistance on the order of $5 \text{ k}\Omega/\square$. The thickness was shown to be between 50 and 800 nm. An inductor was printed and shown to have an inductance on the order of $1 \mu\text{H}$. The ink was shown to adhere well to paper, glass, polyimide, and Nomex © substrates.

5.4 Significance of Research

As previously stated, research in the printed electronics field is important to the USAF and to the DoD. Outside of the DoD, research is being conducted by public and private institutions. For devices to be built using deposition by printer, the basic materials used to print must first be characterized. This research provides an electrical and physical characterization of the research grade Brewer Science © CNT-based inks designed for ink jet and aerosol jet printers. Such a characterization provides specific data which can be used in the future while designing printed electronic devices. Data pertaining to the physical characteristics allow designers to determine how the material can be mechanically incorporated into the planned device. Data pertaining to the electrical characteristics allow designers to determine how the deposited material will affect the performance and efficiency of the circuit.

5.5 Recommendations for Future Research

We recommend that future research be conducted in this area. However, future research should be conducted only once any inks being used are fully understood. The lack of information provided by Brewer Science © for this research prevented the identification of the ink's thickening in transport. Possible topics on which to focus include the following. The electrical and physical characterization of CNT-based inks which include only semiconducting or metallic CNTs, and not a mixture of both; Methods for deposition of CNT-based inks via aerosol jet printers; How the electrical and physical properties of a CNT-based ink change when the ink is blended with a metallic ink; How the process of printing affects the CNTs themselves; for instance, does it break them down into carbon powder?; The electrical and physical characteristics of CNT-based inks manufactured by companies other than Brewer Science; The electrical and physical characteristics of CNT-based circuits constructed using additive manufacturing techniques other than ink jet printing; The effect of pneumatic printing using an aerosol jet printer; The method

and manner in which current flows through deposited CNTs; Methods for decreasing the minimum possible feature size for the Dimatix printer; Thickness measurements of printed ink using atomic force microscopy; Methods for deposition of screen printed CNT-based ink; Printing on a conductive substrate with a thin oxide coat in order to accurately test the effect of an electric field bias on the S-parameters; Characterization of undiluted ink from Brewer Science ©; Characterization method for inspecting CNT inks arriving from outside sources.

5.6 Summary

This chapter presented the conclusions and recommendations for our CNT-based ink research. Section 5.2 presented answers to the investigative questions. Section 5.3 presented the conclusion of the research presented in previous chapters. Section 5.4 described the significance of this research to the USAF, DoD, and the private sector. Section 5.5 described the future research recommended by the authors of this research.

Bibliography

- [1] “Air force research lab awards optomec contract to advance fully printed transistor technology,” Dec. 2013.
- [2] “New nano-bio manufacturing consortium releases first request for proposals on human performance monitoring and biomarkers,” July 2013.
- [3] C. M. Bartsch, “Conversation on brewer science characterization estimates.” Personal Communication, October 2014.
- [4] J. Phillips, *Physics for Scientists and Engineers with Modern Physics*. Upper Saddle River, NJ: Prentice Hall, 4th ed., 2009.
- [5] T. Chowdhury and J. F. Rohan, *Syntheses and Applications of Carbon Nanotubes and Their Composites*. INTECH, 1st ed., 2013.
- [6] W. A. Zisman, “Relations of the equilibrium contact angle to liquid and solid constitution,” *Contact Angle, Wettability, and Adhesion*, pp. 1–51, January 1964.
- [7] “Printed, flexible, and organic electronics: A growing opportunity,” July 2014.
- [8] X. Wang, Q. Li, J. Xie, Z. Jin, J. Wang, Y. Li, K. Jiang, and S. Fan, “Fabrication of Ultralong and Electrically Uniform Single-Walled Carbon Nanotubes on Clean Substrates,” *Nano Letters*, vol. 9, pp. 3137–3141, Sept. 2009.
- [9] S. Gullapalli and M. S. Wong, “Nanotechnology: A guide to nano-objects.,” *Chemical Engineering Progressl*, pp. 28–32, 2011.
- [10] F. Li, H. M. Cheng, S. Bai, G. Su, and M. S. Dresselhaus, “Tensile strength of single-walled carbon nanotubes directly measured from their macroscopic ropes,” *Applied Physics Letters*, September 2000.
- [11] U. of Oxford Department of Physics, “Carbon nanotubes,” 2011.
- [12] J.-C. Charlier, X. Blase, and S. Roche, “Electronic and transport properties of nanotubes,” *Reviews of Modern Physics*, 2007.
- [13] S. Hong and S. Myung, “Nanotube electronics: A flexible approach to mobility,” *Nature Nanotechnology*.
- [14] E. Pop, D. Mann, Q. Wang, K. Goodson, and H. Dai, “Thermal conductance of an individual single-wall carbon nanotube above room temperature,” *NanoLetters*.

- [15] K. Mizunoa, J. Ishiib, H. Kishidac, Y. Hayamizua, S. Yasudaa, D. N. Futabaa, M. Yumuraa, and K. Hataa, “A black body absorber from vertically aligned single-walled carbon nanotubes,” *Proceedings of the National Academy of Sciences of the United States of America*.
- [16] A. Loiseau, *Understanding Carbon Nanotubes: From Basics to Applications*. Springer Science and Business Media, 1st ed., 2006.
- [17] F. Ogletree, “Enhanced thermal transport at covalently functionalized carbon nanotube array interfaces,” *Nature Communications*, 2014.
- [18] J. Robertson, “Low temperature growth of ultra-high mass density carbon nanotube forests on conductive supports,” *Applied Physics Letters*, August 2013.
- [19] N. Srivastava and K. Banerjee, “Performance analysis of carbon nanotube interconnects for vlsi applications,” in *Computer-Aided Design, ICCAD-2005*, 2005.
- [20] A. Javey, “Highly sensitive electronic whiskers based on patterned carbon nanotube and silver nanoparticle composite films,” *Phys Org*, 2014.
- [21] A. Javey, “Photoactuators and motors based on carbon nanotubes with selective chirality distributions,” *Nature Communications*, 2014.
- [22] H. Dai, “Narrow graphene nanoribbons from carbon nanotubes,” *Nature*, 2010.
- [23] A. V. Talyzin, I. V. Anoshkin, A. V. Krasheninnikov, R. M. Nieminen, A. G. Nasibulin, H. Jiang, and E. I. Kauppinen, “Synthesis of graphene nanoribbons encapsulated in single-walled carbon nanotubes,” *Nano Letters*, August 2011.
- [24] L. Jiao, “Narrow graphene nanoribbons from carbon nanotubes,” *Nature*, no. 458, pp. 877–8780, 2009.
- [25] D. V. Kosynkin, “Longitudinal unzipping of carbon nanotubes to form graphene nanoribbons,” *Nature*, no. 458, pp. 872–876, 2009.
- [26] S. E. Ready, “3d printed electronics.,” *NIP29 / Digital Fabrication 2013*, October 2013.
- [27] G. L. Whiting, “Printed circuits and sensing systems,” *American Vacuum Society 60th International Symposium and Exhibition*, October 2013.
- [28] R. S. Aga, J. P. Lombardi, C. M. Bartsch, and E. M. Heckman, “Performance of a printed photodetector on a paper substrate.,” *IEEE Photonics Technology Letters*, January 2014.
- [29] E. M. Heckman, “Biotronics for defense.,” *SPIE Professional*, April 2011.

- [30] C. Yumusak, T. B. Singh, N. S. Sariciftci, and J. G. Grote, “Bio-organic field effect transistors based on crosslinked deoxyribonucleic acid (dna) gate dielectric.,” *Applied Physics Letters*, 2009.
- [31] B. Singh, N. S. Sariciftci, J. G. Grote, and F. K. Hopkins, “Bio-organic-semiconductor-field-effect-transistor based on deoxyribonucleic acid gate dielectric.,” *Journal of Applied Physics*, 2006.
- [32] M. Jung, J. Kim, J. Noh, N. Lim, C. Lim, G. Lee, J. Kim, G. Cho, J. M. Tour, K. Jung, and H. Kang, “All-printed and roll-to-roll-printable 13.56-mhz-operated 1-bit rf tag on plastic foils.,” *Electron Devices, IEEE Transactions on*, 2010.
- [33] G. Orecchini, L. Yang, M. M. Tentzeris, and L. Roselli, “Wearable battery-free active paper-printed rfid tag with human-energy scavenger.,” in *Microwave Symposium Digest (MTT),IEEE MTT-S International*, 2011.
- [34] M. O’Connor, “Printed-electronics rfid tags debut,” *RFID Journal*, August 2010.
- [35] R. Williams, “RFID tag,” 2013.
- [36] J. Song, J. Kim, Y. Yoon, B. Choi, J. Kim, and C. Han, “Inkjet printing of single-walled carbon nanotubes and electrical characterization of the line pattern,” *Nanotechnology*, vol. 19, 2008.
- [37] C. Bartsch and J. Lombardi, “Conversation on ink-jet printing techniques.” Personal Communication, April 2014.
- [38] S. Merilampi, T. Laine-Ma, and P. Ruuskanen, “The characterization of electrically conductive silver ink patterns on flexible substrates,” *Microelectronics Reliability*, vol. 49, no. 7, 2009.
- [39] M. Hedges and A. B. Marin, “3d aerosol jet printing - adding electronics functionality to rp/rm,” in *DDMC 2012 Conference*, 2012.
- [40] J. Lombardi, “Conversation on brewer scientific inks.” Personal Communication, April 2014.
- [41] R. P. Tortorich and J. W. Choi, “Inkjet printing of carbon nanotubes,” *Nanomaterials*, vol. 3, 2013.
- [42] P. Beecher, P. Servati, A. Rozhin, A. Colli, V. Scardaci, S. Pisana, T. Hasan, A. J. Flewitt, J. Robertson, and G. W. Hsieh, “Ink-jet printing of carbon nanotube thin film transistors,” *Journal of Applied Physics*, vol. 102, 2007.
- [43] W. R. Small and M. in het Panhuis, “Inkjet printing of transparent, electrically conducting single-walled carbon-nanotube composites.,” *Small*, pp. 1500–1503, September 2007.

- [44] F. Smits, “Measurement of sheet resistivities with the four-point probe,” *Bell System Technical Journal*, vol. 34, pp. 711–718, May 1958.
- [45] K. E. W. Jr., M. Y. Lanzerotti, C. M. Bartsch, and J. P. L. III, “Characterization of electrical and physical properties of single-walled carbon nanotube ink,” in *National Aerospace and Electronics Conference*, 2013.
- [46] Vessels42, “Four-point.” Internet, July 2007. Public Domain Photograph.
- [47] F. M. Smits, “Measurement of sheet resistivities with the four-point probe,” *The Bell System Technical Journal*.
- [48] D. Schroder, *Semiconductor material and device characterization*. Piscataway NJ; Hoboken N.J.: IEEE Press; Wiley, 3rd ed., 2006.
- [49] D. E. Johnson, J. R. Johnson, J. L. Hilburn, and P. D. Scott, *Electric Circuit Analysis*. Prentice Hall, 3rd ed., 1997.
- [50] S. Jahn, “Coplanar waveguides,” 2007.

REPORT DOCUMENTATION PAGE

*Form Approved
OMB No. 0704-0188*

The public reporting burden for this collection of information is estimated to average 1 hour per response, including the time for reviewing instructions, searching existing data sources, gathering and maintaining the data needed, and completing and reviewing the collection of information. Send comments regarding this burden estimate or any other aspect of this collection of information, including suggestions for reducing this burden to Department of Defense, Washington Headquarters Services, Directorate for Information Operations and Reports (0704-0188), 1215 Jefferson Davis Highway, Suite 1204, Arlington, VA 22202-4302. Respondents should be aware that notwithstanding any other provision of law, no person shall be subject to any penalty for failing to comply with a collection of information if it does not display a currently valid OMB control number. PLEASE DO NOT RETURN YOUR FORM TO THE ABOVE ADDRESS.

| | | | |
|---|--|--|--|
| 1. REPORT DATE (DD-MM-YYYY) 26-03-2015 | 2. REPORT TYPE Master's Thesis | 3. DATES COVERED (From — To) Oct 2013-Mar 2015 | |
| 4. TITLE AND SUBTITLE Electrical and Physical Property Characterization of Single Walled Carbon Nanotube Ink for Flexible Printed Electronics | | 5a. CONTRACT NUMBER 5b. GRANT NUMBER 5c. PROGRAM ELEMENT NUMBER 5d. PROJECT NUMBER JON14G150, JON15P150 5e. TASK NUMBER 5f. WORK UNIT NUMBER | |
| 6. AUTHOR(S) Warner Jr, Kristian E., Second Lieutenant, USAF | | 7. PERFORMING ORGANIZATION NAME(S) AND ADDRESS(ES) Air Force Institute of Technology Graduate School of Engineering and Management (AFIT/EN) 2950 Hobson Way WPAFB, OH 45433-7765 | 8. PERFORMING ORGANIZATION REPORT NUMBER AFIT-ENG-MS-15-M-066 |
| 9. SPONSORING / MONITORING AGENCY NAME(S) AND ADDRESS(ES) Air Force Research Laboratory Mr. Bradley Paul 2241 Avionics Circle WPAFB, OH 43433-7322 Bradley.Paul@us.af.mil (937) 528-8706 | | 10. SPONSOR/MONITOR'S ACRONYM(S) AFRL/RYDI | |
| | | 11. SPONSOR/MONITOR'S REPORT NUMBER(S) | |
| 12. DISTRIBUTION / AVAILABILITY STATEMENT DISTRIBUTION STATEMENT A: APPROVED FOR PUBLIC RELEASE; DISTRIBUTION UNLIMITED | | | |
| 13. SUPPLEMENTARY NOTES This work is declared a work of the U.S. Government and is not subject to copyright protection in the United States. | | | |
| 14. ABSTRACT This research presents a method of characterizing single-walled carbon nanotube (SWCNT) ink. This research also examines the results of our characterization efforts. First, the process of ink jet printing SWCNT ink onto organic and inorganic substrates is discussed. Next, the tests for measuring sheet resistance, conductance, inductance, adherence, thickness, roll-off, and S-parameters of the ink are described. Results and findings of the research are presented. The SWCNT ink created by Brewer Science © is shown to be an effective material for additive manufacturing using an aerosol jet printer, but not an inkjet printer. The ink is shown to have a sheet resistance on the order of $5 \text{ k}\Omega/\square$. The thickness is shown to be between 50 and 800 nm. An inductor is printed and shown to have an inductance on the order of $1 \mu\text{H}$. Future research directions are discussed, including the additional characterization of SWCNT ink. | | | |
| 15. SUBJECT TERMS Printed Electronics, Carbon Nanotube, Ink Characterization, Brewer Science | | | |
| 16. SECURITY CLASSIFICATION OF: a. REPORT U b. ABSTRACT U c. THIS PAGE U | | 17. LIMITATION OF ABSTRACT UU | 18. NUMBER OF PAGES 92 |
| | | 19a. NAME OF RESPONSIBLE PERSON Maj Derrick Langley (ENG) | 19b. TELEPHONE NUMBER (include area code) (937)785-3636 x6165 Derrick.Langley@AFIT.edu |